# Simplification and Analysis of Models of Calcium Dynamics Based on $IP_3$-Sensitive Calcium Channel Kinetics

Yuanhua Tang,* John L. Stephenson,* and Hans G. Othmer‡
*Department of Physiology and Biophysics, Cornell University Medical College, New York, New York 10021, and ‡Department of Mathematics, University of Utah, Salt Lake City, Utah 84112 USA

ABSTRACT We study the models for calcium (Ca) dynamics developed in earlier studies, in each of which the key component is the kinetics of intracellular inositol-1,4,5-trisphosphate-sensitive Ca channels. After rapidly equilibrating steps are eliminated, the channel kinetics in these models are represented by a single differential equation that is linear in the state of the channel. In the reduced kinetic model, the graph of the steady-state fraction of conducting channels as a function of $\log_{10}$(Ca) is a bell-shaped curve. Dynamically, a step increase in inositol-1,4,5-trisphosphate induces an incremental increase in the fraction of conducting channels, whereas a step increase in Ca can either potentiate or inhibit channel activation, depending on the Ca level before and after the increase. The relationships among these models are discussed, and experimental tests to distinguish between them are given. Under certain conditions the models for intracellular calcium dynamics are reduced to the singular perturbed form $\epsilon dx/d\tau = f(x, y, p)$, $dy/d\tau = g(x, y, p)$. Phase-plane analysis is applied to a generic form of these simplified models to show how different types of Ca response, such as excitability, oscillations, and a sustained elevation of Ca, can arise. The generic model can also be used to study frequency encoding of hormonal stimuli, to determine the conditions for stable traveling Ca waves, and to understand the effect of channel properties on the wave speed.

## INTRODUCTION

### $IP_3$-sensitive intracellular Ca channels

Cytoplasmic calcium ($Ca_i$) is a universal second messenger for regulation of many cellular components and processes, including muscle contraction, secretion, membrane permeability, and fertilization. The extracellular signals for such processes can be hormones, growth factors, neurotransmitters, membrane depolarization, or physical signals such as light or shear stresses. One mode of regulation of $Ca_i$ is by means of the activation and inactivation of Ca channels between the cytoplasm and intracellular Ca stores, which are either the endoplasmic reticulum (ER) in nonmuscle cells or the sarcoplasmic reticulum (SR) in muscle cells. These channels are of two major types, inositol-1,4,5-trisphosphate ($IP_3$)-sensitive Ca channels ($IP_3R$) and ryanodine-sensitive Ca channels (RyR), but there may be many subtypes of these two types, depending on the cell type in question.

Experiments in which $IP_3R$ are inserted into lipid bilayers show that $IP_3$ upregulates the channel activity (Watras et al., 1991), whereas Ca has both a positive and a negative effect on the channel activity. At steady state the graph of the fraction of channels open versus $\log_{10}([Ca_i])$, which we denote $p$Ca, is a bell-shaped curve (Bezprozvanny et al., 1991). Moreover, activation of channels at low Ca concentrations and inhibition at high concentrations are seen in a variety of intact cell types (Zhao et al., 1990; Wakui and Petersen, 1990; Parker and Ivorra, 1990; Meyer and Stryer, 1990).

### Theoretical problems in Ca dynamics

Several theoretical questions arise from the study of intracellular Ca dynamics, one of which relates to the mechanism of frequency encoding. In the study of Ca dynamics in hepatocytes in response to vasopressin stimuli, Woods et al. (1986) found that, over the range of 200 nM to 1 $\mu$M in the hormone concentration, stimuli evoke repetitive spikes in the intracellular Ca concentration rather than simply elevating the level of Ca. Moreover, they found that as the hormone concentration was raised, the frequency of spiking increased but the amplitude remained essentially constant. Thus the continuously graded (analog) extracellular hormone signal was converted into a frequency-encoded digital signal (the number of Ca spikes). Similar dynamic behavior has been found in a large number of cell types since then and has led to the suggestion that Ca spiking and frequency encoding must have a physiological role (Meyer and Stryer, 1991). In secretory cells such as pancreatic acinar cells, this frequency can determine the secretion rate of digestive enzymes and fluid (Kasai, 1995).

Another significant aspect of intracellular Ca dynamics is that the response in many cells is spatially inhomogeneous. In a variety of cell types, waves of Ca release propagate across the cell in response to hormonal or other stimuli. For instance, in *Xenopus laevis* oocytes, penetration of a sperm into the egg triggers a localized increase in $Ca_i$ that propagates away from the point of entry at approximately 10

*Received for publication 30 June 1995 and in final form 9 October 1995.*
Address reprint requests to Dr. Yuanhua Tang, Department of Physiology and Biophysics, Cornell University Medical College; New York, NY 10021. Tel.: 212-746-6361; Fax: 212-746-8690; E-mail: tang@figaro.med.cornell.edu.
© 1996 by the Biophysical Society
0006-3495/96/01/246/18 $2.00

$\mu$m/s, inducing cortical contraction, meiosis, and structural rearrangement (Nuccitelli, 1991). Because some of the $IP_3$-sensitive calcium stores in *Xenopus* oocytes are localized at the animal pole (Lupu-Meiri et al., 1988; Berridge, 1990), spatiotemporal propagation of $Ca_i$ waves is essential for inducing the entire cell to respond to a localized stimulus. Spatially inhomogeneous waves such as spiral waves and target patterns can also be triggered locally along the cortical surface of *Xenopus* oocytes (Lechleiter et al., 1991; Lechleiter and Clapham, 1992), though the physiological significance of these artificially induced waves is unknown. In hepatocytes Ca oscillations appear to originate from a single locus and propagate across the cell. The initiation site seems to be relatively constant in a given cell, even for different agonists. When hepatocytes are treated with phenylephrine, followed by washout and restimulation with vasopressin, Ca waves originate from the same site. The speed of the waves in hepatocytes is typically 20–25 $\mu$m/s (Thomas et al., 1991). These cells are polarized to a degree, and a variety of receptors are known to be concentrated at the sinusoidal membrane, which may account for the hypersensitivity of this region to activating signals. The physiological significance of nonuniform spatiotemporal patterns of Ca is probably clearest in eosinophils during chemotaxis. In these cells an intracellular Ca gradient is responsible for the initial polarization of a homogeneous cell and for the subsequent change in polarity as the cell responds to extracellular chemical attractants (Fay et al., 1995).

Spatial variations in calcium are important at the supracellular level as well. For instance, Ca waves may be used to synchronize large cell assemblies such as ciliated epithelial cells (Meyer, 1991), and diffusion of $IP_3$ through gap junctions appears to be necessary for the propagation of these waves (Boitano et al., 1992). In the mammalian brain, it is found that Ca waves can spread from a single astrocyte into a population of astrocytes in vitro (Nedergaad, 1994; Sneyd et al., 1994). The slowly spreading Ca waves of ~20 $\mu$m/s may be correlated with the phenomenon of spreading depression in vivo (Gorelova and Bures, 1983).

## Kinetic models for $IP_3R$

Many mathematical models for Ca dynamics in systems involving $IP_3R$ have been proposed (Ehrenstein and FitzHugh, 1986; Meyer and Stryer, 1988; Goldbeter et al., 1990). Models that were proposed before the work of Bezprozvanny et al. (1991) usually involve feedback regulation of Ca on $IP_3$ production with the result that $IP_3$ oscillates whenever Ca does. The model of Ehrenstein and FitzHugh (1986) and that of Meyer and Stryer (1988) belong to this category. Wakui et al. (1989) showed that $IP_3$ oscillations are not required for Ca oscillations because the nonhydrolyzable $IP_3$ analog $IP_3S_3$ also induces Ca oscillations. The experimental findings of Bezprozvanny et al. (1991) gave rise to a new class of Ca dynamics models that center around the kinetics of $IP_3R$ (De Young and Keizer, 1992; Othmer and Tang, 1993; Atri et al., 1993; Bezprozvanny and Ehrlich, 1994). In view of the aforementioned experimental data on channel activities, these models of $IP_3R$ assume three regulatory sites on the channel complex, one for $IP_3$ and two for Ca. Of the two Ca regulatory sites, one is positive regulatory (activating) and the other negative regulatory (inhibitory). In all the models Ca binding to the positive regulatory site is a fast process compared with that of negative binding. These models predict that the steady-state fraction of open channels as a function of $p$Ca is a bell-shaped curve with the optimal fraction open at physiological Ca concentrations.

The kinetic model of $IP_3R$ proposed by De Young and Keizer assumes that the ligands can bind to any unoccupied site on the receptor irrespective of the binding status of other sites. The Othmer–Tang model, on the other hand, assumes a sequential binding scheme: $IP_3$ has to bind at the $IP_3$ site before Ca can bind to the channel. In addition, the binding of Ca to the two Ca sites is also ordered: Ca has to bind to the positive regulatory site before it can bind to the negative site. The most general scheme is to assume state-dependent binding to each site with distinct parameters for each of the binding and release steps, and both the De Young–Keizer model and the Othmer–Tang model can be obtained by a special choice of parameters in such a scheme. Another variation on this general scheme assumes that the binding and/or release of the regulators is state independent, which leads to the Atri–Amundson–Clapham–Sneyd model. The Bezprozvanny–Ehrlich model is a variation of the Othmer–Tang sequential binding scheme, which incorporates an additional transition to the open state. In this model $IP_3R$ with the $IP_3$ and positive Ca sites occupied is assumed to be a closed state, and the channel undergoes a fast transition from this state to the open state. In addition, a slight inhibitory effect of ER Ca on the channel is incorporated into the model. Numerical simulations using these models show that they are all capable of predicting experimental results qualitatively. Among all these models, the Othmer–Tang model has the least number of channel states and kinetic parameters, yet it adequately explains the experimentally observed channel kinetics (Bezprozvanny and Ehrlich, 1994).

## Mathematical models for Ca dynamics and their simplification

Each of the above models for $IP_3R$ can be incorporated into a model for intracellular Ca dynamics for those cells for which $IP_3R$ are the only type of intracellular Ca channels, and this has been done for all but the Bezprozvanny–Ehrlich model. The typical cell types modeled are hepatocytes, *Xenopus* oocytes, and endothelial cells. A schematic diagram of the components involved in these models is shown in Fig. 1. There is a transmembrane receptor responsive to hormonal or other agonist signals that transduces the stim-

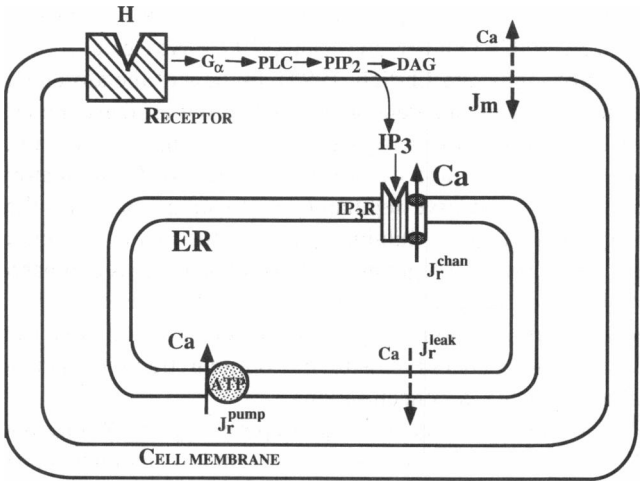


FIGURE 1 Schematic diagram of Ca regulation in cells with $IP_3R$. An extracellular agonist binds to a receptor which then activates a G-protein. The activated G-protein in turn activates PLC, which breaks down phosphatidyl inositol 4,5-biphosphate ($PIP_2$) to generate $IP_3$ and diacylglycerol (DAG). $IP_3$ diffuses into the cytoplasm and binds with $IP_3$-sensitive Ca channels ($IP_3R$) in the ER membrane. Ca is released through $IP_3R$ and through a nonspecific leakage, and it is pumped into the ER by Ca pumps in the ER membrane. In general, there is also a Ca flux, $J_m$, across the cytoplasm membrane.

ulatory signal to a G-protein. The activated G-protein in turn activates phospholipase C (PLC), and activated PLC catalyzes the hydrolysis of a membrane phospholipid, phosphatidyl inositol 4,5-bisphosphate, thereby generating two messengers, $IP_3$ and diacylglycerol. $IP_3$ is water soluble and diffuses into the cytoplasm. On binding with $IP_3R$, it activates the Ca channels and induces the release of stored Ca from the ER into the cytoplasm. In addition, there is leakage of Ca from the ER into the cytoplasm. The Ca-ATPase on the ER membrane is primarily responsible for pumping Ca back into the ER. Cytoplasmic $IP_3$ is short lived: after a few seconds it is degraded and recycled into the membrane through specific pathways. Cells may also exchange Ca with the extracellular medium through unspecified leaks or special protein-mediated processes.

Each of the models can simulate certain aspects of the experimental behavior of these cells. For example, the Othmer–Tang model can predict excitability and oscillations, depending on the hormonal concentration. When the hormonal level exceeds a certain value, sustained stable oscillations are replaced by temporally damped oscillations around a relatively high $Ca_i$ level. A further increase in hormonal stimulation leads to an overdamped response around a high sustained Ca level. When spatial aspects are introduced, the Othmer–Tang model generates various types of traveling wave.

Even though the above-mentioned models are simple and are suitable for numerical studies, they are generally too complex for analytical studies aimed at understanding frequency encoding (Tang and Othmer, 1995) and traveling waves. Past experience with models for excitable systems has shown that simplifications can often reveal the essential dynamical behavior in a model, and can suggest critical experimental tests of its applicability and limitations. For instance, the Hodgkin-Huxley (1952) model for the transmembrane potential in nerve cells has been simplified to two equations (the Fitzhugh-Nagumo system) and studied in detail mathematically, leading to the first proof of the existence of traveling wave solutions in the reduced system and advancing our understanding of excitable media. In this spirit, Keizer and De Young (1994) and Li and Rinzel (1994) have reduced the De Young–Keizer model to different forms of a two-equation system. The equations in the reduced Keizer–De Young system govern the dynamics of $IP_3R$, whereas the other components of the Ca dynamics are assumed to relax instantaneously. In the Li–Rinzel reduction, one equation is for $IP_3R$ kinetics and the other is for Ca release from and uptake into the ER.

We extend this work by showing that all of the aforementioned kinetic schemes for $IP_3R$ kinetics can be reduced to a single equation of the Hodgkin–Huxley form:

$$\frac{dy}{d\tau} = \frac{y_\infty - y}{\tau_y}, \tag{1}$$

where $y$ is the fraction of channels with Ca bound at the inhibitory site. Thus we obtain a standard form for a wide class of models, and thereby we show that they differ only in the dependence of $y_\infty$, $\tau_y$, and the fraction of activated states on Ca and $IP_3$. We show that the models proposed by Othmer and Tang (1993) and by Bezprozvanny and Ehrlich (1994) are in fact equivalent to within the choice of the parameter values. We also provide a simplification for the De Young–Keizer model that is different from both the De Young–Keizer reduction and the Li–Rinzel reduction. Finally, we show how the phenomenological equations used by Atri et al. (1993) can be obtained through a kinetic-based derivation.

When the total amount of Ca in the cytoplasm–ER complex is conserved, it is shown that all the models for intracellular Ca dynamics can be reduced to a generic two-equation form. With the assumption that the channel gating equation is slow compared with the Ca release from and the uptake into the ER, the reduced two-equation system has one slow variable and one fast variable. Phase-plane analysis and singular perturbation techniques are applied to a generic model to show how excitability, oscillations, frequency encoding, and sustained elevations of $Ca_i$ arise as the $IP_3$ concentration varies. The influence on Ca dynamics of a slow exchange of Ca between the cytoplasm and the extracellular medium can also be studied in the reduced model.

## SIMPLIFICATION OF KINETIC MODELS FOR $IP_3R$

### Othmer–Tang model

Othmer and Tang (1993) propose a four-state model for the $IP_3$-sensitive Ca channel in which the transitions between the different states occur according to the

following scheme:

$$R \underset{l_{-0}}{\overset{l_0 I}{\rightleftarrows}} RI \underset{l_{-1}}{\overset{l_1 C}{\rightleftarrows}} RIC^+ \underset{l_{-2}}{\overset{l_2 C}{\rightleftarrows}} RIC^+C^-. \quad (2)$$

Here $I$ denotes $IP_3$ and $C$ denotes $Ca_i$, $R$ denotes the bare $IP_3$ receptor and $RI$ the receptor with $IP_3$ bound, $RIC^+$ denotes $RI$ with a Ca bound at the activating site, and $RIC^+C^-$ denotes $RIC^+$ with an additional Ca bound at the inhibitory sites. Let $C_c = [Ca_i]$, $I_c = [IP_3]$, $s_{000} = [R]/[R]_T$, $s_{100} = [RI]/[R]_T$, $s_{110} = [RIC^+]/[R]_T$, and $s_{111} = [RIC^+C^-]/[R]_T$, where $[R]_T$ denotes the total concentration of $IP_3$ receptors. Then the governing equations are

$$\begin{aligned}
\frac{ds_{000}}{dt} &= -l_0 I_c s_{000} + l_{-0} s_{100}, \\
\frac{ds_{100}}{dt} &= -(l_{-0} + l_1 C_c) s_{100} + l_0 I_c s_{000} + l_{-1} s_{110}, \quad (3) \\
\frac{ds_{111}}{dt} &= l_2 C_c s_{110} - l_{-2} s_{111},
\end{aligned}$$

and $s_{000} + s_{100} + s_{110} + s_{111} = 1$. To simplify the channel kinetics, we assume that the binding of $IP_3$ to the receptor and of Ca to the positive regulatory site of the receptor is fast and that the binding of Ca to the negative regulatory site is slow. Experimentally it is found that the $IP_3$-induced channel opening occurs within hundreds of milliseconds for $IP_3$ in the nanomolar to micromolar range and decreases as the $IP_3$ level increases (Wootton et al., 1995). The time course of binding/release of $IP_3$ to the channel is not detectable on the time scale of many measurements with an $IP_3$ level in the physiological range (Meyer and Stryer, 1990; Finch et al., 1991). Less is known directly about the speed of Ca binding/release to the activating site on $IP_3R$, which can be measured experimentally by photoreleasing caged Ca in permeabilized cells. For the RyR in cardiac muscle the time scale is of order milliseconds (Gyorke and Fill, 1993). If the time scales of Ca binding to the activating site and $IP_3$ binding/release are at least 10 times faster than the time scale of Ca binding/release at

**TABLE 1 Definition of dimensionless parameters and their values**

| Parameter | Definition | DeY-K | O-T | Generic | B-E | B | AACS |
|---|---|---|---|---|---|---|---|
| $\epsilon$ | $l_{-2} \cdot s$ | 0.21 | 0.21 | 0.018 | 0.8 | 0.8 | |
| $\alpha_1$ | $(1 + \nu_r) \cdot g_1 \cdot s$ | 0.13 | 0.12 | 0.003 | | | |
| $\alpha_2$ | $(1 + \nu_r) P_r^{chan} \cdot s$ | 7.11 | 22.92 | 4.27 | | | |
| $\alpha_3$ | $\nu_r P_r^{max}/C_M \cdot s$ | 0.5326 | 5.449 | 0.64 | | | |
| $\alpha_4$ | $K_r^M/C_M$ | 0.05924 | 0.32 | 0.019 | | | 0.1 |
| $n$ | Hill Coefficient | 2 | 4 | 2 | | | 1 |
| $\beta_0$ | $\frac{l_{-0}}{l_0 I_c}$ | $0.13/I_c$ | $0.667/I_c$ | $0.8/I_c$ | Unknown | Unknown | Unknown |
| $\beta_1$ | $\frac{l_{-1}}{l_1 C_M}$ | 47.78 | 0.0705 | 0.077 | 0.2 | | 0.7 |
| $\beta_2$ | $\frac{l_{-2}}{l_2 C_M}$ | 0.622 | 0.0749 | 0.064 | 0.2 | | |
| $\beta_3$ | $\frac{l_{-3}}{l_3 I_c}$ | $943.4/I_c$ | | | | | |
| $\beta_4$ | $\frac{l_{-4}}{l_4 C_M}$ | 85.6 | | | | | |
| $\beta_5$ | $l_{-4}/l_{-2}$ | 137.62 | | | | | |
| $\beta_r$ | $\frac{l_r z_r}{l_{-2}}$ | | | | $228.8 z_r$ | 0 | |
| $\beta_t$ | $\frac{l_t}{l_{-t} + l_r z_r}$ | | | | $\frac{25.2}{224 + 184 z_r}$ | 0.1125 | |
| $\bar{\beta}_1$ | $\frac{l_{-1}/l_1 C_M}{1 + l_t/l_{-t}}$ | | | | | 0.1152 | |
| $\bar{\beta}_2$ | $\frac{l_{-2}}{l_2 C_M}(1 + l_t/l_{-t})$ | | | | | 0.1426 | |
| $\hat{\beta}_2$ | $\sqrt{\frac{l_{-2}}{\hat{l}_2}} \cdot C_M$ | | | | | | 0.7 |
| $C_M$ | Scaling concentration | 1.688 $\mu$M | 1.56 $\mu$M | | 1 $\mu$M | 1.56 $\mu$M | 1 $\mu$M |

Here B stands for the Bezprozvanny model, B-E for the Bezprozvanny–Ehrlich model, DeY-K for the De Young–Keizer model; O-T for the Othmer-Tang model, AACS for the Atri–Amundson–Clapham–Sneyd model, and Generic for the parameters used in the analysis sections. For AACS, basal rates of $IP_3R$ transitions are not included.

the inhibitory site, then, to a good approximation, we can assume that the fast dynamics have equilibrated on the slow time scale, i.e., $\dot{s}_{000} = \dot{s}_{100} = 0$ (Kijima and Kijima, 1983). This argument can be made rigorous by applying singular perturbation techniques to the differential equations (Eq. 3). A more general and rigorous reduction of first-order kinetic systems of this type based on singular perturbation and graph-theoretic techniques will be given elsewhere (Tikhonov, 1952).

Let us introduce dimensionless dissociation parameters $\beta_i$, $i = 0, 1, 2$ for the three binding/release steps in the kinetic transitions, with $\beta_0(I_c) = l_{-0}/(l_0 I)$ and $\beta_i = l_{-i}/(l_i C_M)$, $i = 1, 2$, and $C_M$ is a reference $Ca_i$ concentration. For later purposes, we define the dimensionless Ca concentration $x = C_c/C_M$, the dimensionless fraction of channels in the inhibited state $y = s_{111}$, and the dimensionless time $\tau = l_{-2}t$ (cf. Table 1). Then on the slow time scale

$$s_{000} = \frac{\beta_0(I_c)\beta_1(1-y)}{x + \beta_1(1 + \beta_0(I_c))},$$

$$s_{100} = \frac{\beta_1(1-y)}{x + \beta_1(1 + \beta_0(I_c))}, \tag{4}$$

$$s_{110} = \frac{x(1-y)}{x + \beta_1(1 + \beta_0(I_c))},$$

and the equation for the slow variable is

$$\frac{dy}{d\tau} = -y + \frac{x^2}{\beta_2[x + \beta_1(1 + \beta_0(I_c))]}(1-y). \tag{5}$$

This can be written in the equivalent Hodgkin–Huxley form (Eq. 1), wherein $\tau_y$ and $y_\infty$ are given in Table 2.

## Bezprozvanny–Ehrlich model

Bezprozvanny and Ehrlich (1994) proposed a model for $IP_3R$ kinetics based on their experiments with $IP_3R$ inserted into lipid bilayers. This model is a variation of the Othmer–Tang (1993) model with the introduction of an additional state $R^*IC^+$ for the channel. The kinetic scheme for the channel is depicted in the following diagram. (The model published in Bezprozvanny and Ehrlich (1994) differs slightly from the scheme represented here, in that it does not have the $IP_3$ binding step. The symbols for the kinetic constants are also changed to make the usage of symbols consistent throughout this paper.)

$$\begin{array}{ccccccc} & & & & R^*IC^+ & & \\ & & & & l_t \uparrow\downarrow l_{-t} & \searrow l_r \cdot z_r & \\ & & l_0 I & & l_1 C & & l_2 C \\ R & \rightleftarrows & RI & \rightleftarrows & RIC^+ & \rightleftarrows & RIC^+C^-. \\ & & l_{-0} & & l_{-1} & & l_{-2} \end{array} \tag{6}$$

In this model $RIC^+$, the activated state, is not conducting; only the transition to the state $R^*IC^+$ makes it conducting. To account for the inhibitory effect of intraluminal Ca on the channel observed in the experiments, Bezprozvanny and Ehrlich (1994) also introduced a direct transition from the open state to the inhibited state. This transition is mediated by Ca in a specific location on the cytoplasmic side near the conducting pore. According to the argument in Bezprozvanny and Ehrlich (1994), the Ca concentration at this location is proportional to the fraction $z_r$ of all divalent ions *inside* the ER that is Ca.

Let $s^*_{110}$ be the fraction of channels in the state $R^*IC^+$. As before we assume that binding of $IP_3$ and Ca to the positive site on $IP_3R$ is fast. In addition we assume that the transi-

**TABLE 2** $\tau_y$ **and** $y_\infty$ **in simplified kinetic models for** $IP_3R$

| Model | $\tau_y$ | $y_\infty$ |
|---|---|---|
| O-T | $\dfrac{\beta_2 x + \beta_1\beta_2(1 + \beta_0(I_c))}{x^2 + \beta_2 x + \beta_1\beta_2(1 + \beta_0(I_c))}$ | $\dfrac{x^2}{x^2 + \beta_2 x + \beta_1\beta_2(1 + \beta_0(I_c))}$ |
| B-E | $\dfrac{\beta_2(1 + \beta_t)x + \beta_1\beta_2(1 + \beta_0(I_c))}{x^2 + \beta_2(1 + \beta_t + \beta_r\beta_t)x + \beta_1\beta_2(1 + \beta_0(I_c))}$ | $\dfrac{x^2 + \beta_2\beta_r\beta_t}{x^2 + \beta_2(1 + \beta_t + \beta_r\beta_t)x + \beta_1\beta_2(1 + \beta_0(I_c))}$ |
| B | $\dfrac{\bar{\beta}_2 x + \bar{\beta}_1\bar{\beta}_2(1 + \beta_0(I_c))}{x^2 + \bar{\beta}_2 x + \bar{\beta}_1\bar{\beta}_2(1 + \beta_0(I_c))}$ | $\dfrac{x^2}{x^2 + \bar{\beta}_2 x + \bar{\beta}_1\bar{\beta}_2(1 + \beta_0(I_c))}$ |
| DeY-K | $\dfrac{\beta_2\beta_4[1 + \beta_3(I_c)][1 + \beta_0(I_c)]}{ax + b}$ | $\dfrac{[1 + \beta_3(I_c)][\beta_4 + \beta_2\beta_5\beta_0(I_c)]x}{ax + b}$ |
| DeY-K (indep.) | $\dfrac{\beta_2}{x + \beta_2}$ | $\dfrac{x}{x + \beta_2}$ |
| AACS (original) | 2.0 | $\dfrac{C_c^2}{C_c^2 + k_2^2}$ |
| AACS (rederived) | $\dfrac{(\hat{\beta}_2)^2}{x^2 + (\hat{\beta}_2)^2}$ | $\dfrac{x^2}{x^2 + (\hat{\beta}_2)^2}$ |

Here DeY-K (indep.) stands for a variation of the De Young–Keizer model with the assumption that the binding of regulatory factors ($I$, $C^+$, $C^-$) is state independent; AACS (original) stands for the original Atri–Amundson–Clapham–Sneyd model, in which $1 - y_n$ corresponds to the gating variable $n$ in their original notation; and AACS (rederived) stands for the rederived Atri–Amundson–Clapham–Sneyd model based on the kinetic scheme presented in Eq. 18. $ax + b = [1 + \beta_3(I_c)][\beta_4 + \beta_2\beta_5\beta_0(I_c)]x + \beta_2\beta_4[1 + \beta_0(I_c)][1 + \beta_5\beta_3(I_c)]$ in the DeY-K formulas. See text for more details of each model.

tions between $RIC^+$ and $R^*IC^+$ are fast. The latter assumption is consistent with the choice of parameter values in Bezprozvanny and Ehrlich (1994) for the transition steps. Even with $Ca_i$ at 1 $\mu$M, the slowest process, which is the transition between $RIC^+$ and $RIC^+C^-$, is more than sixfold slower than transitions between $RIC^+$ and $R^*IC^+$. Thus, the equations for the rapidly equilibrating species are

$$\begin{aligned}\frac{ds_{000}}{dt} &= -l_0 I_c s_{000} + l_{-0} s_{100},\\ \frac{ds_{100}}{dt} &= -(l_{-0} + l_{-1} + l_2 C_c + l_t) s_{100} + l_0 I_c s_{000}\\ &\quad + l_1 C_c s_{100} + l_{-2} s_{111} + l_{-t} s^*_{110},\\ \frac{ds^*_{110}}{dt} &= l_3 s_{110} - (l_{-t} + l_r z_r) s^*_{110},\end{aligned} \tag{7}$$

and $s_{000} + s_{100} + s_{110} + s^*_{110} + s_{111} = 1$. At a quasi-steady state these yield

$$\begin{aligned}s_{000} &= \frac{\beta_0(I_c)\beta_1(1-y)}{(1+\beta_t)x + \beta_1(1+\beta_0(I_c))},\\ s_{100} &= \frac{\beta_1(1-y)}{(1+\beta_t)x + \beta_1(1+\beta_0(I_c))},\\ s_{110} &= \frac{x(1-y)}{(1+\beta_t)x + \beta_1(1+\beta_0(I_c))},\\ s^*_{110} &= \frac{\beta_t x(1-y)}{(1+\beta_t)x + \beta_1(1+\beta_0(I_c))},\end{aligned} \tag{8}$$

where the definition of $\beta_i$ ($i = 0, 1, 2$) is as before. The new parameters are $\beta_r = l_r z_r / l_{-2}$ and $\beta_t = l_t/(l_{-t} + l_r z_r)$. We set $y = s_{111}$ as before and find that the equation for the slow dynamics is

$$\frac{dy}{d\tau} = -y + \frac{x(x + \beta_2\beta_r\beta_t)}{\beta_2[\beta_1(1+\beta_0(I_c)) + (1+\beta_t)x]}(1-y). \tag{9}$$

Note that the dependence of $y$ on $x$ involves a linear term as well as a quadratic term in the numerator.

The values of the dimensionless parameters that appear in these equations are given in Table 1. According to these estimates the inhibitory step that is ER Ca dependent is never very significant compared with the inactivation step $R^*IC^+ \rightarrow RIC^+$. Under physiological conditions the transition from $R^*IC^+$ to $RIC^+C^-$ is ~20% of the transition from $R^*IC^+$ to $RIC^+$ (Bezprozvanny and Ehrlich, 1994). Thus, to a first approximation, the transition of $R^*IC^+$ directly to the inhibited state can be ignored. In this case, the Bezprozvanny–Ehrlich model reduces to a model proposed by Bezprozvanny (1994) in which the inhibition of ER Ca on the channel is absent, i.e., in Eq. 9 $\beta_r = 0$ and $\beta_t = l_t/l_{-t}$.

The improvement of the Bezprozvanny model over the Othmer–Tang model lies in the introduction of the additional state $R^*IC^+$. Incorporation of this state resolves an issue not treated by other models, which is that the experimentally-observed fraction of channels in the conducting state is usually below 10% (Bezprozvanny et al., 1991), even though the fraction of the channels in the activated state can be much higher in the mathematical models (Othmer and Tang, 1993; De Young and Keizer, 1992).

To clarify the relationship between the Bezprozvanny model and the Othmer–Tang model, let us denote the combined fraction of channels in the states $RIC^+$ and $R^*IC^+$ by $\bar{s}_{110}$, i.e., $\bar{s}_{110} = s_{110} + s^*_{110}$. By introducing the new dimensionless parameters $\bar{\beta}_1 = \beta_1/(1+\beta_t)$ and $\bar{\beta}_2 = \beta_2(1+\beta_t)$, we obtain the following relations for the steady-state fractions:

$$\begin{aligned}s_{000} &= \frac{\beta_0(I_c)\bar{\beta}_1(1-y)}{x + \bar{\beta}_1(1+\beta_0(I_c))},\\ s_{100} &= \frac{\bar{\beta}_1(1-y)}{x + \bar{\beta}_1(1+\beta_0(I_c))},\\ \bar{s}_{110} &= \frac{x(1-y)}{x + \bar{\beta}_1(1+\beta_0(I_c))}.\end{aligned} \tag{10}$$

Eq. 9 can now be rewritten as

$$\frac{dy}{d\tau} = -y + \frac{x^2}{\bar{\beta}_2[x + \bar{\beta}_1(1+\beta_0(I_c))]}(1-y). \tag{11}$$

Thus, under the assumption that the transition between the activated state and the open state is fast compared with that of channel inhibition by Ca and channel recovery, the equations for the Bezprozvanny model become identical to Eqs. 4 and 5 modulo the change in the definition of the parameters. The distribution of $\bar{s}_{110}$ within the two substates, which is needed in the Ca balance equations, is

$$s_{110} = \frac{\bar{s}_{110}}{1+\beta_t}, \qquad s^*_{110} = \frac{\bar{s}_{110}}{1+\beta_t}. \tag{12}$$

## De Young–Keizer model

De Young and Keizer proposed the first kinetic model for $IP_3P$ (De Young and Keizer, 1992). In their model, regulatory factors ($IP_3$ and Ca) can bind to the channel complex in a state-dependent manner. The proposed scheme of channel regulation is presented in the following notation, with modified symbols for the coefficients of kinetic transitions to make the symbols used within this paper consistent:

$$\begin{array}{ccccccccc} & & l_{-0} & & l_{-1} & & l_0 I & & l_1 C & \\ RIC^+ & \rightleftarrows & & RC^+ & & R & & RI & & RIC^+ \\ & & l_0 I & & l_1 C & & l_{-0} & & l_{-1} & \\ l_4 C \uparrow\downarrow l_{-4} & & l_{-3} & l_2 C \uparrow\downarrow l_{-2} & l_{-1} & l_2 C \uparrow\downarrow l_{-2} & l_3 I & l_4 C \uparrow\downarrow l_{-4} & l_1 C & l_4 C \uparrow\downarrow l_{-4} \\ RIC^+C^- & \rightleftarrows & l_3 I & RC^+C^- & \rightleftarrows & RC^- & \rightleftarrows & RIC^- & \rightleftarrows & RIC^+C^-. \\ & & & & & & l_{-3} & & l_{-1} & \end{array} \tag{13}$$

For the choice of parameters used in De Young and Keizer (1992) the binding/release of $IP_3$ and of positive regulatory Ca to the channel complex are fast processes compared with

that of inhibitory Ca binding/release. With this set of kinetic parameters the channel states can be separated into two groups: Group I, the uninhibited group $s_{000}$, $s_{010}$, $s_{100}$, $s_{110}$ (the top group in Eq. 13), and Group II, the inhibited group $s_{001}$, $s_{101}$, $s_{111}$, $s_{011}$ (the bottom group in Eq. 13). Within each group the transitions among the states are fast. We assume that on the slow time scale a quasi-steady state has been reached within each group. Let $y = s_{001} + s_{101} + s_{111} + s_{011}$; then $1 - y = s_{000} + s_{010} + s_{100} + s_{110}$. Ignoring the slow transitions between the two groups, the differential equations for species in the uninhibited group are

$$\begin{aligned}
\frac{ds_{000}}{dt} &= -(l_0 I_c + l_1 C_c)s_{000} + l_{-0}s_{100} + l_{-1}s_{010},\\
\frac{ds_{100}}{dt} &= -(l_{-0} + l_1 C_c)s_{100} + l_0 I_c s_{000} + l_{-1}s_{110},\\
\frac{ds_{010}}{dt} &= -(l_{-1} + l_0 I_c)s_{010} + l_1 C_c s_{000} + l_{-0}s_{110},\\
\frac{ds_{110}}{dt} &= -(l_{-0} + l_{-1})s_{110} + l_0 I_c s_{010} + l_1 C_c s_{100}.
\end{aligned} \tag{14}$$

By setting $\dot{s}_{000} = \dot{s}_{100} = \dot{s}_{010} = 0$ and using the conservation equation for this subgroup, which holds exactly when the rates for the vertical transitions are zero, we get

$$\begin{aligned}
s_{000} &= \frac{\beta_0(I_c)\beta_1(1-y)}{(1+\beta_0(I_c))(x+\beta_1)},\\
s_{100} &= \frac{\beta_1(1-y)}{(1+\beta_0(I_c))(x+\beta_1)},\\
s_{010} &= \frac{\beta_0(I_c)x(1-y)}{(1+\beta_0(I_c))(x+\beta_1)},\\
s_{110} &= \frac{x(1-y)}{(1+\beta_0(I_c))(x+\beta_1)},
\end{aligned} \tag{15}$$

where $\beta_i$ ($i = 0, 1, 2$) are as before. Similarly, the quasi-steady-state distribution of the channels in the inhibited group is

$$s_{001} = \frac{\beta_3(I_c)\beta_1 y}{(1+\beta_3(I_c))(x+\beta_1)}, \quad s_{101} = \frac{\beta_1 y}{(1+\beta_3(I_c))(x+\beta_1)},$$

$$s_{011} = \frac{\beta_3(I_c)xy}{(1+\beta_3(I_c))(x+\beta_1)}, \quad s_{111} = \frac{xy}{(1+\beta_3(I_c))(x+\beta_1)},$$

where $\beta_3(I_c) = l_{-3}/(l_3 I_c)$. The equation for the slow variable of the channel kinetics to within terms that are small is

$$\begin{aligned}
\frac{dy}{dt} &= -l_{-4}(s_{001} + s_{011}) - l_{-2}(s_{101} + s_{111})\\
&\quad + l_4 C_c(s_{000} + s_{010}) + l_2 C_c(s_{100} + s_{110}).
\end{aligned} \tag{16}$$

The corresponding dimensionless equation is

$$\frac{dy}{d\tau} = -\frac{(1+\beta_5\beta_3(I_c))}{1+\beta_3(I_c)}y + \frac{(\beta_4 + \beta_5\beta_0(I_c)\beta_2)x}{\beta_2\beta_4(1+\beta_0(I_c))}(1-y),$$

where $\beta_4 = l_{-4}/(l_4 C_M)$, $\beta_5 = l_{-4}/l_{-2}$. This reduced form of the De Young–Keizer model for $IP_3R$ differs from the Li–Rinzel reduction slightly (Li and Rinzel, 1994). In our reduction, the conservation condition $\sum_{i,j,k=0}^{1} s_{ijk} = 1$ is satisfied exactly, whereas in the Li–Rinzel reduction it is satisfied only approximately. In fact, the departure from the conservation equation in their reduction is of order $O(\delta)$, where $\delta \sim 0.1$ by their estimate.

One important variation of the De Young–Keizer model is to assume that the rate of binding is independent of the state of the channel complex. The resulting scheme is very similar to that in Eq. 13 but with $l_3 = l_0$, $l_{-3} = l_{-0}$ and $l_4 = l_2$, $l_{-4} = l_{-2}$. This modified model has the same number of channel states as the original De Young–Keizer model but has the same number of parameters as the Othmer–Tang model. To get the simplified kinetic equation, we set $\beta_3(I_c) = \beta_0(I_c)$, $\beta_4 = \beta_2$, and $\beta_5 = 1$ in Eq. 17 and find that

$$\begin{aligned}
\frac{dy}{d\tau} &= -y + \frac{x}{\beta_2}(1-y),\\
s_{110} &= \frac{x(1-y)}{(1+\beta_0(I_c))(x+\beta_1)}.
\end{aligned} \tag{17}$$

The most general scheme in which binding/release are state-dependent is obtained by assigning different kinetic parameters to each of the steps in Eq. 13. In addition, the four subunits within the channel complex of $IP_3R$ may interact with one another cooperatively (Watras et al., 1991). To study the cooperativity, a more general scheme than Eq. 13 is needed, one example of which has been studied in Tang (1993).

## Atri–Amundson–Clapham–Sneyd model

Atri et al. (1993) studied a phenomenological model based on a single gating equation for the dynamics of $IP_3R$. As in the other models, $IP_3R$ is assumed to have three regulatory binding sites, an $IP_3$ site, a positive regulatory Ca site, and a negative regulatory Ca site. The binding of the regulatory factors to their sites is in effect assumed to be state independent. Unlike in the foregoing three models, Atri et al. (1993) assume that the negative site requires the cooperative binding of two Ca ions to close the channel. Here we rederive the channel equation based on the following detailed kinetic scheme:

$$\begin{array}{ccccccccc}
RIC^+ & \underset{l_0 I}{\overset{l_{-0}}{\rightleftarrows}} & RC^+ & \underset{l_1 C}{\overset{l_{-1}}{\rightleftarrows}} & R & \underset{l_{-0}}{\overset{l_0 I}{\rightleftarrows}} & RI & \underset{l_{-1}}{\overset{l_1 C}{\rightleftarrows}} & RIC^+\\
\hat{k}C^2 \Updownarrow l_{-2} & & \hat{k}C^2 \Updownarrow l_{-2} & & \hat{k}C^2 \Updownarrow l_{-2} & & \hat{k}C^2 \Updownarrow l_{-2} & & \hat{k}C^2 \Updownarrow l_{-2}\\
RIC^+(C^2)^- & \underset{l_0 I}{\overset{l_{-0}}{\rightleftarrows}} & RC^+(C^2)^- & \underset{l_1 C}{\overset{l_{-1}}{\rightleftarrows}} & R(C^2)^- & \underset{l_{-0}}{\overset{l_0 I}{\rightleftarrows}} & RI(C^2)^- & \underset{l_{-1}}{\overset{l_1 C}{\rightleftarrows}} & RIC^+(C^2)^-.
\end{array} \tag{18}$$

Here $(C^2)^-$ corresponds to two Ca ions bound to the inhibitory site. Let $p_i$, $i = 1, 2, 3$ denote the fraction of channels in the group of states that with $IP_3$ bound, that with stimulatory Ca bound, and that *without* inhibitory Ca bound, respectively; then $p_1 = \sum_{i,j=0}^{1} s_{1ij}$, $p_2 = \sum_{i,j=0}^{1} s_{i1j}$, $p_3 = \sum_{i,j=0}^{1} s_{ij0}$, where the usage of $s_{ijk}$ is as before. The differential equations for the combined subpopulations are

$$\begin{aligned} \frac{dp_1}{dt} &= l_0 I_c (1 - p_1) - l_{-0} p_1, \\ \frac{dp_2}{dt} &= l_1 C_c (1 - p_2) - l_{-1} p_2, \\ \frac{d(1 - p_3)}{dt} &= \hat{l}_2 C_c^2 p_3 - l_{-2}(1 - p_3). \end{aligned} \tag{19}$$

The steady state of these equations is

$$\begin{aligned} p_1 &= \frac{1}{1 + \beta_0(I_c)}, \qquad p_2 = \frac{x}{x + \beta_1}, \\ p_3 &= 1 - \frac{x^2}{x^2 + (\hat{\beta}_2)^2}, \end{aligned} \tag{20}$$

with $\beta_i$, $i = 0, 1$ defined as before and $(\hat{\beta}_2)^2 = l_{-2} C_M^2 / \hat{l}_2$. The channel kinetics can be approximated by a single differential equation for the slow variable $1 - p_3$, and, if we use the same symbol as for the previous models for $IP_3R$ (i.e., $\tau = l_{-2} t$, $y = 1 - p_3$), we find that

$$\begin{aligned} \frac{dy}{d\tau} &= -y + \frac{x^2}{(\hat{\beta}_2)^2}(1 - y), \\ s_{110} &= \frac{x(1 - y)}{(1 + \beta_0(I_c))(x + \beta_1)}. \end{aligned} \tag{21}$$

This equation is the same as Eq. 17 for the state-independent version of the De Young–Keizer model, except that $\beta_2$ is replaced by $(\hat{\beta}_2)^2$ and $x$ appears quadratically in the $y$ equation. If only one Ca binds to the negative regulatory site instead of two, Eqs. 21 and 17 become identical, as do the kinetic schemes.

Instead of postulating a detailed transition scheme, Atri et al. (1993) assumed phenomenologically that the fractions of the channels for the subgroups satisfy

$$\begin{aligned} p_1 &= \mu_0 + \frac{\mu_1 I_c}{k_\mu + I_c}, \qquad p_2 = b + \frac{V_1 C_c}{k_1 + C_c}, \\ p_3 &= 1 - \frac{C_c^2}{k_2^2 + C_c^2}, \end{aligned} \tag{22}$$

where $k_\mu$, $k_1$, $k_2$ are the dissociation constants, $\mu_1$, $V_1$ the maximal proportion of the ligand binding, and $\mu_0$, $b$ the rates of basal transition with no ligand binding required. The dimensional channel dynamics are given by

$$\begin{aligned} \tau_n \frac{dy_n}{dt} &= \frac{C_c^2}{k_2^2 + C_c^2} - y_n, \\ s_{110} &= \left(\mu_0 + \frac{\mu_1 I_c}{k_\mu + I_c}\right)\left(b + \frac{V_1 C_c}{k_1 + C_c}\right)(1 - y_n), \end{aligned} \tag{23}$$

where $y_n$ is the gating variable and $\tau_n$ is its time constant. $y_n$ corresponds to $1 - n$ in Atri et al. (1993). Some symbols are changed from the original paper for consistency with the usage in this paper.

The formulas for the subpopulations that we rederive are similar to the equations postulated in Atri et al. (1993), but there are some important differences: i) there is no basal transition between $s_{0ij}$ and $s_{1ij}$ and between $s_{i0j}$ and $s_{i1j}$. As a result, for $i = 1, 2$, $p_i = 0$ when ligand concentrations are 0 and $p_i = 1$ when they are infinity. Those derived by Atri et al. (1993) do not satisfy these conditions. ii) Equations 16 and 18 for channel gating in Atri et al. (1993) are replaced by a gating equation (Eq. 21) based on a rigorous reduction. In making this replacement we find that the time constant $\tau_y$ for channel inhibition and recovery depends on the Ca concentration, whereas Atri et al. (1993) assume that $\tau_n$ is constant.

The values of the nondimensionalized parameters for the kinetic models are given in Table 1, and the values for the corresponding dimensional parameters are given in Table 3. Table 1 also gives the parameter values for the Bezprozvanny scheme based on the symbols used in Eq. 11. For ease of comparison, the steady-state fractions of activated and inhibited channels and the relaxation time for the Hodgkin–Huxley form (Eq. 1) of each model is given in Table 2. In the following section we study the channel dynamics, using the Othmer–Tang model for $IP_3R$ as the example.

## ANALYSIS OF CHANNEL KINETICS IN THE SIMPLIFIED MODELS

### Steady-state channel behavior

To study the channel dynamics under conditions that simulate experiments on reconstituted channels in lipid layers, we assume that the Ca concentration is a given function of time (Bezprozvanny et al., 1991). The steady-state fraction of activated and inhibited channels is (cf. Table 2)

$$\begin{aligned} s_{110} &= \frac{\beta_2 x}{x^2 + \beta_2 x + \beta_1 \beta_2 (1 + \beta_0(I_c))}, \\ y_\infty &= \frac{x^2}{x^2 + \beta_2 x + \beta_1 \beta_2 (1 + \beta_0(I_c))}. \end{aligned} \tag{24}$$

Elementary analysis of these equations shows that

- $s_{110}(0) = \lim_{x \to \infty} s_{110}(x) = 0$;
- $s_{110}$ is a concave function of $x$ with a single maximum that occurs at $x^{max} = \sqrt{\beta_1 \beta_2 (1 + \beta_0(I_c))}$ and at this value

$$s_{110}^{max} = \frac{\sqrt{\beta_1 \beta_2 (1 + \beta_0(I_c))}}{2\beta_1 (1 + \beta_0(I_c)) + \sqrt{\beta_1 \beta_2 (1 + \beta_0(I_c))}};$$

- $y_\infty$ is a monotonic function of $x$, $y_\infty(0) = 0$, $0 \le y_\infty < 1$, and $\lim_{x \to \infty} y_\infty(x) = 1$.

The graph of $s_{110}$ versus $p$Ca is a bell-shaped curve that varies with $IP_3$, as is shown in Fig. 2. It should be noted that the curves are not symmetric for $p$Ca in the range $[-2, 1]$: the fraction of channels open at $p\text{Ca} = -2$ is larger than that at $p\text{Ca} = 1$. This agrees with the experimental result of Bezprozvanny et al. (1991) somewhat better than the corresponding result for the De Young–Keizer model (De Young and Keizer, 1992). As the $IP_3$ level increases, the fraction open at fixed Ca increases, and the concentration at which the maximum occurs shifts leftward. This is different from the prediction made by De Young and Keizer (1992), who state that the peak should shift to the right with increasing $IP_3$ levels. The Atri–Amundson–Clapham–Sneyd model predicts that the Ca concentration at which the maximum occurs is independent of $IP_3$ levels. These predictions can be tested with the experimental protocol of Bezprozvanny et al. (1991). Of particular importance is to determine whether the binding of $IP_3$ and Ca is sequential.

Further insight into the steady-state channel behavior can be obtained by fixing Ca and determining the effect of varying $IP_3$. As $\beta_0 = l_{-0}/(l_0 l_c)$, one sees from Eq. 24 that the fraction of channels that is activated increases monotonically as the $IP_3$ level increases (cf. Fig. 3 *a*). An experimental result from Watras et al. (1991) is shown for comparison in Fig. 3 *b*.

## Time-dependent responses

Experimentally it is found that a step increase in $C_c$ can have a predominantly activating effect on $IP_3R$; it can involve both activation and adaptation; or it can have an essentially inhibitory effect, depending on the existing level of Ca and the size of the step increase (Zhao et al., 1990; Wakui and Petersen, 1990; Parker and Ivorra, 1990; Meyer and Stryer, 1990). As the following computational results show, these effects can be reproduced by the simplified model. In Fig. 4 *a* we show the predicted channel response to the experimental protocol of step increases of $C_c$ obtained by photolysis of caged Ca

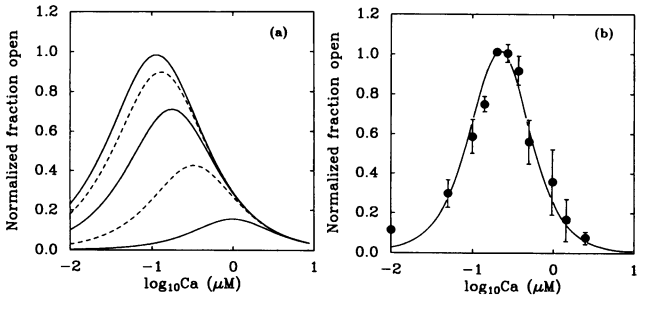


FIGURE 2 Steady-state fraction of activated channels as a function of $\log_{10}$ Ca in the Othmer–Tang model for $IP_3R$. $IP_3$ levels are (from the lowermost curve upward): 0.01 μM (*solid*); 0.1 μM (*dashed*); 0.5 μM (*solid*); 2.0 μM (*dashed*); and 10.0 μM (*solid*). The maximum fraction of activated channels is 31%. (*b*) Experimental result from Bezprozvanny et al. (1991) (with permission). The $IP_3$ concentration is 2 μM, and the maximum percentage of channels open is 15%.

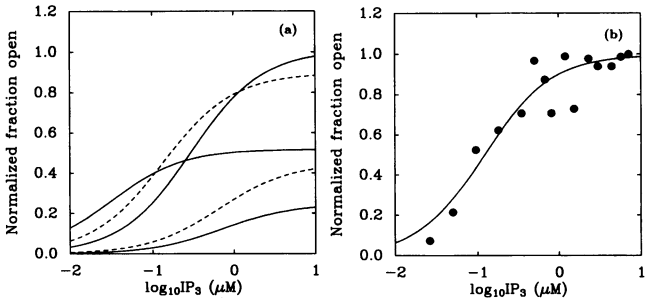


FIGURE 3 Predicted steady-state fraction of activated channels as a function of the $IP_3$ concentration at different levels of cytoplasmic Ca. Ca levels are (from lowermost curve at the left upward) 0.01 μM (*solid*), 0.02 μM (*dashed*); 0.1 μM (*solid*); 0.2 μM (*dashed*); and 0.5 μM (*solid*). The maximum fraction of activated channels is 31%. (*b*) Experimental result from Watras et al. (1991) (with permission). *cis* Ca is 0.1 μM, and the maximum fraction of channels open is 14%.

on the *cis* side of reconstituted $IP_3R$ in lipid bilayers. Initially the fraction of activated channels is at the steady-state level for $C_c = 0.01$ μM and $I_c = 0.1$ μM. When $C_c$ is stepped up to 0.1 μM, the fraction of channels activated increases significantly, and the adaptation, which we define as the fractional return of the open channels to the prestimulus level, is minimal. As $C_c$ is further increased to 0.5 μM, the steady-state incremental increase in activation is small, whereas the effect of adaptation is more prominent. Furthermore, the rate at which activated channels make the transition to the inhibited state is much higher than in the previous step. When $C_c$ is further increased to 1 μM at 10 min, the inhibitory effect of Ca on the channels becomes dominant, although a small increase in the fraction of activated channels is seen in the first few seconds of the response.

The temporal signature of the response to a step in $C_c$ represents a balance between activation and inhibition of the channels. At low $C_c$ the former dominates, but at higher $C_c$ inhibition dominates. An increase of $C_c$ to levels higher than

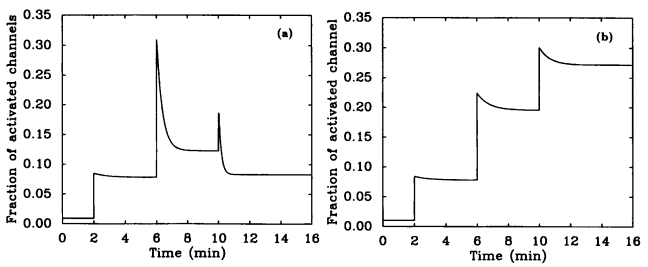


FIGURE 4 Temporal behavior of the fraction of activated channels in response to step changes in *cis* Ca and the $IP_3$ concentration in the simplified Othmer–Tang model. (*a*) Channel activation, adaptation, and inhibition in response to multiple step increases in *cis* Ca. Ca levels are 0.01 μM for $t \in [0, 2]$, 0.1 μM for $t \in [2, 6]$, 0.5 μM for $t \in [6, 10]$, and 1.0 μM thereafter. $IP_3$ is fixed at 0.1 μM throughout. (*b*) Incremental increases in the fraction of activated channels in response to stepwise increases in $IP_3$. $IP_3$ levels are 0.01 μM for $t \in [0, 2]$, 0.1 μM for $t \in [2, 6]$, 0.5 μM for $t \in [6, 10]$, and 2.0 μM thereafter. *cis* Ca is fixed at 0.1 μM throughout.

$C_M \cdot x^{max}$ will always have an inhibitory effect on the fraction of channels opened, because of the bell-shaped nature of the steady-state fraction of channels open as a function of $C_c$. The steady-state levels of the activated fractions in Fig. 4 *a* correspond to discrete points on the bell-shaped curve in Fig. 2 *a* with $I_c = 0.1$ $\mu$M and $C_c =$ 0.01, 0.1, 0.5, and 1 $\mu$M.

Another aspect of $IP_3R$ dynamics, incremental Ca release, is revealed under step increases of $IP_3$ (Fig. 4 *b*). As $I_c$ is increased the fraction of channels activated increases. This incremental increase with increasing $IP_3$ stimuli has been observed in various experiments and has been labeled quantal Ca release (Irvine, 1990; Oldershaw et al., 1991). Inasmuch as there is no experimental evidence of a minimum or quantal Ca-releasing vesicle inside either the ER or SR, the terminology seems inappropriate. The incremental release that is due to additional $IP_3$ has a dynamic and a steady phase, and in the latter the steady state corresponds to a unique point in Fig. 3 *b*.

Experiments on Ca release through intact $IP_3R$ have also been done with Ca-ATPase inhibited and $C_c$ and $I_c$ controlled (Taylor and Potter, 1990; Hirose and Iino, 1994). Under these conditions, the foregoing results suggest that Ca release from the Ca store will be biphasic following a step increase in $I_c$. If we suppose that the leakage from the store is negligible and that the step increase of $IP_3$ is at $t = 0$, then the Ca concentration in the store at time $t$, $C_r(t)$, is

$$C_r(t) = C_c + (C_r(0) - C_c)\exp(-P_r^{chan} s_{110}(t)\, t), \quad (25)$$

where $P_r^{chan}$ is a constant determined by $IP_3R$ density and the conductance of open channels. Because $s_{110}(t)$ undergoes a step increase followed by exponential decay to a higher steady state (cf. Fig. 4 *b*), $C_r(t) - C_c$ will decrease at a nonexponential rate in the initial phase, as is observed (Taylor and Potter, 1990). As $t$ increases, $s_{110}$ relaxes to a new steady-state level, and as a result the difference between ER and cytoplasmic Ca decays exponentially in the second phase. In this phase the slope of a semilogarithmic plot of $C_r(t) - C_c$ versus $t$ can be used to estimate $P_r^{chan}$ if $s_{110}$ can be determined by other methods. For example, $P_r^{chan}$ can be estimated at $\sim$1.04 $s^{-1}$ for Ca stores in vascular smooth muscle cells under the assumption that $s_{110} \sim$ 1% for $I_c = 0.1$ $\mu$M and a very low $C_c$ (cf. Fig. 4 of Hirose and Iino (1994), where $C_c$ is strongly buffered). Of course $P_r^{chan}$ varies between cell types because of differences in channel density and the channel subtype. The speed of the transition from the first phase to the second phase is determined by both the $IP_3$ and the Ca level in the medium. Increasing either $C_c$ or $I_c$ will shorten the duration of the first phase. Increasing $I_c$ will also decrease $t_{1/2}$, the time for half-depletion of the store, whereas increasing $C_c$ can either increase or decrease it.

The simplified equations for channel dynamics predict both the qualitative and quantitative behavior of the other transition schemes as well. Thus these simplifications can be used to test experimentally the applicability of each scheme. The various shifts of $x^{max}$ on the bell-shaped curve predicted in response to $IP_3$ changes is one example, but there are additional differences. For example, the independent-binding version of $IP_3R$ kinetics predicts that the off rate of channel gating ($x/\beta_2$ in the independent scheme with only one Ca bound to the inhibitory site on $IP_3R$, or $x^2/(\hat{\beta}_2)^2$ in the Atri–Amundson–Clapham–Sneyd scheme with the cooperative binding of two Ca to this site) is independent of the $IP_3$ level, whereas the sequential binding scheme (Othmer–Tang model) predicts that it should depend on the $IP_3$ level in the form $x^2/(\beta_2[x + \beta_1(1 + \beta_0(I_c)])$. The dependence of $\tau_y$ on $C_c$ as shown here for the Atri–Amundson–Clapham–Sneyd model, which contrasts with the assumed Ca independence of $\tau_n$ in Atri et al. (1993), can also be tested.

The simplified models also provide an avenue for easier parameter estimation. For example, $\beta_0$, $\beta_1$, and $\beta_2$ in the Othmer–Tang model for $IP_3R$ can be estimated based on the measurement of $x^{max}$ and $s_{110}^{max}$ and the dependence of $s_{110}$ on $IP_3$. The parameter $l_{-2}$ can then be determined based on the dynamical response of channel adaptation to a single-step Ca increase. Alternatively, $\beta_2$ and $l_{-2}$ can be estimated from data on sequential-step Ca increases.

## SIMPLIFIED MODELS FOR INTRACELLULAR Ca DYNAMICS

A mathematical model for $Ca_i$ dynamics in cells having $IP_3R$, based on the components shown in Fig. 1, was proposed in Othmer and Tang (1993). We denote by $J_r$ and $J_m$ the Ca fluxes across the ER and cytoplasmic membranes, respectively. $J_r$ has several components that are indicated with the superscripts leak, chan, and pump to denote Ca leakage, the channel flux, and the flux that is due to the active pump. Under the assumption that both the cytoplasm and the ER are homogeneous media, the differential equations for the calcium concentrations are

$$\begin{aligned} \frac{dC_c}{dt} &= \nu_r(J_r^{leak} + J_r^{chan} - J_r^{pump}) + J_m, \\ \frac{dC_r}{dt} &= -J_r^{leak} - J_r^{chan} + J_r^{pump}, \end{aligned} \quad (26)$$

where $\nu_r$ is the ratio of the ER volume to that of the cytoplasm. The ATP-dependent pump that moves cytosolic Ca into the ER can be modeled by $J_r^{pump} = P_r^{max}\,(C_c^n/C_c^n + (K_r^M)^n)$, where $P_r^{max}$ is the maximal pumping rate, $K_r^M$ the Michaelis–Menten constant, and $n$ the Hill coefficient. Because the ER membrane is very permeable to sodium and potassium ions, it is reasonable to assume that it does not support a potential difference. Thus the leakage rate of Ca is simply $J_r^{leak} = P_r^{leak}\,(C_r - C_c)$, where $P_r^{leak}$ is the leakage permeability coefficient. The $IP_3R$-mediated Ca flux from the ER to the cytoplasm should also be proportional to the concentration of channels that are in the open state; thus,

$J_r^{chan} = P_r^{chan} s_{110}(C_r - C_c)$, where $P_r^{chan}$ is the channel permeability coefficient. Depending on the specific cell type, $J_m$ may include components that are due to leakage, to a channel-mediated flux, and to an active transport process mediated by the Ca pump and the Na/Ca exchanger. The active flux driven by Ca-TAPase in the cytoplasmic membrane is similar to that in the ER membrane (Gmaj and Murer, 1988). Other fluxes in the cytoplasmic membrane are more complicated because of the involvement of the membrane potential and ionic species other than Ca, a detailed description of which can be found in Tang and Stephenson (1995).

Let $C_M$ denote the mean Ca concentration in the cell, which is defined by $v_r C_r + C_c = (1 + v_r)C_M$. The differential equations for intracellular Ca dynamics can be written in the form

$$\frac{dC_M}{dt} = \frac{J_m}{1 + v_r},$$

$$\frac{dC_c}{dt} = (1 + v_r)(P_r^{leak} + P_r^{chan} s_{110})(C_M - C_c) - P_r^{max} \frac{C_c^n}{C_c^n + (K_r^M)^n} + J_m. \quad (27)$$

For the study of Ca excitability, oscillations, and traveling waves in many cell types, such as deutosome eggs, hepatocytes, endothelial cells, and kidney cells, Ca exchange with the extracellular medium is relatively small. Most of the experiments exploring the intracellular Ca dynamics in these cell types can be carried out in Ca-free media or with high extracellular EGTA concentrations, at least for an initial period of several minutes. In these cells, blocking PLC or applying thapsigargin completely blocks the $Ca_i$ response to stimulatory hormones (Koster et al., 1993; Thastrup et al., 1990). These findings suggest that the exchange of Ca with the extracellular medium is much smaller than the Ca flux across the ER membrane; thus this exchange is not essential for the short-time Ca dynamics as long as the change in $C_M$ on this time scale is small. For these cell types we can drop the term $J_m$ in the second equation of Eq. 27 and treat the contribution of Ca exchange across the cytoplasmic membrane as a slow change in $C_M$ on the time scale of the fast Ca response. As a result we assume hereafter that $C_M$ either is a fixed constant or is a parameter whose value can vary as the result of Ca exchange with extracellular medium but that it is not a dynamical variable.

In dimensionless variables we have the following system for Ca and channel dynamics:

$$\epsilon \frac{dx}{d\tau} = \left(\alpha_1 + \alpha_2 \frac{x(1-y)}{x + \beta_1(1 + \beta_0(I_c))}\right)(1 - x) - \frac{\alpha_3 x^n}{x^n + \alpha_4^n},$$

$$\frac{dy}{d\tau} = -y + \frac{x^2(1-y)}{\beta_2[x + \beta_1(1 + \beta_0(I_c)]}. \quad (28)$$

Here $\epsilon = l_{-2} \cdot s$, $\alpha_1 = (1 + v_r)P_r^{leak} \cdot s$, $\alpha_2 = (1 + v_r)P_r^{chan} \cdot s$, $\alpha_3 = v_r P_r^{max}/C_M$, $\alpha_4 = K_r^M/C_M$, and $s$ is a scale factor for the time, which we set equal to 1 second. The parameter values for this reduced form of Othmer–Tang model are given in Table 1, and the values of the dimensional parameters are given in Table 3.

The treatment of intracellular Ca dynamics in the De Young–Keizer model is very similar to the foregoing, except that $J_r^{chan} = P_r^{chan} s_{110}^3 (C_r - C_c)$. This form is based on the assumption that $IP_3R$ is a tetramer composed of four identical subunits and that the tetramer is in the conducting state only when three of its subunits are in the activated state, irrespective of the state of the fourth subunit. An alternative version of this scheme results from the assumption that the channel is in the conducting state if three of its subunits are in the activated state and the fourth subunit is not in the inhibited state. The open probability is then $(1 - s_{111})s_{110}^3$. It is known experimentally that the subunits in $IP_3R$ interact cooperatively (Watras et al., 1991), but whether the De Young–Keizer model addresses cooperativity adequately should be investigated further. The dimensionless equations for the De Young–Keizer model are

$$\epsilon \frac{dx}{d\tau} = \left(\alpha_1 + \alpha_2 \frac{x^3(1-y)^3}{(1 + \beta_0(I_c))^3(x + \beta_1)^3}\right)(1 - x) - \frac{\alpha_3 x^n}{x^n + \alpha_4^n},$$

$$\frac{dy}{d\tau} = -\frac{(1 + \beta_5\beta_3(I_c))y}{1 + \beta_3(I_c)} + \frac{(\beta_4 + \beta_0(I_c)\beta_2\beta_5)x}{\beta_2\beta_4(1 + \beta_0(I_c))}(1 - y). \quad (29)$$

The values of the dimensionless parameters that appear in these equations are given in Table 1, and the values of the dimensional parameters are given in Table 3.

**TABLE 3 Values of the dimensional parameters**

| Parameter | B-E | DeY-K | O-T |
|---|---|---|---|
| $C_M$ | | 1.688 $\mu$M | 1.56 $\mu$M |
| $K_r^M$ | | 0.1 $\mu$M | 0.5 $\mu$M |
| $P_r^{chan}$ | | 6.0 $s^{-1}$ | 20.5 $s^{-1}$ |
| $P_r^{leak}$ | | 0.11 $s^{-1}$ | 0.1 $s^{-1}$ |
| $P_r^{max}$ | | 4.86 $(\mu M \cdot s)^{-1}$ | 8.5 $(\mu M \cdot s)^{-1}$ |
| $n$ | | 2 | 4 |
| $v_r$ | | 0.185 | 0.185 |
| $l_0$ | Unknown | 400 $(\mu M \cdot s)^{-1}$ | 12.0 $(\mu M \cdot s)^{-1}$ |
| $l_1$ | Unknown | 20 $(\mu M \cdot s)^{-1}$ | 15.0 $(\mu M \cdot \cdot \cdot)^{-1}$ |
| $l_2$ | 4 $\mu M^{-1}$ $s^{-1}$ | 0.2 $(\mu M \cdot s)^{-1}$ | 1.8 $(\mu M \cdot s)^{-1}$ |
| $l_3$ | | 400 $(\mu M \cdot s)^{-1}$ | |
| $l_4$ | | 0.2 $(\mu M \cdot s)^{-1}$ | |
| $l_{-0}$ | Unknown | 52 $s^{-1}$ | 8.0 $s^{-1}$ |
| $l_{-1}$ | 0.2 $\mu M l_1$ | 1646.8 $s^{-1}$ | 1.65 $s^{-1}$ |
| $l_{-2}$ | 0.8 $s^{-1}$ | 0.21 $s^{-1}$ | 0.21 $s^{-1}$ |
| $l_{-3}$ | | $3.7736 \times 10^5$ $s^{-1}$ | |
| $l_{-4}$ | | 28.9 $s^{-1}$ | |
| $l_r$ | 183 $s^{-1}$ | | |
| $l_t$ | 25.2 $s^{-1}$ | | |
| $l_{-t}$ | 224 $s^{-1}$ | | |

B-E stands for the Bezprozvanny–Ehrlich model, DeY-K the De Young–Keizer model, and O-T the Othmer–Tang model.

For the alternative form of the De Young–Keizer model, i.e., assuming independent binding of the regulatory factors, the governing equations are

$$\epsilon\frac{dx}{d\tau} = \alpha_1(1-x) + \alpha_2(1-x)\frac{x^3(1-y)^3}{(1+\beta_0(I_c))^3(x+\beta_1)^3} - \frac{\alpha_3 x^n}{x^n+\alpha_4^2}, \tag{30}$$

$$\frac{dy}{d\tau} = -y + \frac{x}{\beta_2}(1-y).$$

The original model by Atri et al. is already in the two-equation format, but it can also be rederived by use of the new channel gating equation.

## ANALYSIS OF A SIMPLIFIED MODEL

The generic form for the two-equation system derived in the previous section is

$$\epsilon\frac{dx}{d\tau} = f(x, y, p), \qquad \frac{dy}{d\tau} = g(x, y, p), \tag{31}$$

where $\epsilon$ is a positive dimensionless parameter and $p$ is a vector that represents the remainder of the dimensionless parameters. If $\epsilon$ is small, Eq. 31 has the generic form of a nondegenerate system in singular perturbation terminology. The corresponding degenerate system obtained by setting $\epsilon = 0$ is $f(x, y, p) = 0$ and the second equation of Eq. 31. The parameter $\epsilon$ reflects the relative time scale of the channel regulation to that of another process whose time scale is of order $s$. This could for instance be the rate of Ca release or the Ca-ATPase pumping rate. In the case of RyR, $\epsilon$ is typically not small, because channel adaptation occurs on the scale of seconds, which is the same time scale as for Ca release (Gyorke and Fill, 1993). However, in the case of $IP_3R$, $\epsilon$ is small compared with other parameters. For example, the typical oscillation peroid in hepatocytes is of the order of 2–4 min, whereas that for the Ca upstroke is of the order of a few seconds. This clean decoupling of the two processes strongly suggests that the rates of channel inhibition and recovery are at least 10-fold slower than the other components of Ca dynamics. As was suggested earlier, $\epsilon$ can be measured experimentally, and in particular, the channel adaptation and recovery in response to Ca can be investigated experimentally by the use of photolysis of caged Ca (Iino and Endo, 1992; Gyorke and Fill, 1993).

All the models for Ca dynamics with $IP_3R$ predict that the temporal period of oscillations is in the range of 10–20 s (Othmer and Tang, 1993; De Young and Keizer, 1992; Atri et al., 1993), which is much shorter than the periods reported for hepatocytes and endothelial cells (Jacob et al., 1988; Woods et al., 1986). The source of this discrepancy lies in the choice of $l_{-2}$. Here we choose a different value for $l_{-2}$ ($\epsilon$ in dimensionless form) for $IP_3R$ to produce oscillations with a period in the physiological range. We will use the generic parameter values listed in Table 1 for the following analysis. The choice of parameter values is based mainly on the estimates in Othmer and Tang (1993), with the above-mentioned modification and a change of the Hill coefficient from 4 to 2 for the Ca-ATPase.

### Excitability in response to $IP_3R$ and Ca stimuli

To study the calcium dynamics in whole tissue preparations, we have to analyze the system in Eq. 28. Although the simplified system has only two equations, the complexity in the nonlinearity precludes an analytic solution. Thus we will use numerical methods to solve the equation and analyze its behavior in the phase plane as some parameters are varied.

The null clines of the system Eq. 28 are given by

$$y_1(x) = 1 + \frac{x+\beta_1(1+L_0/I_c)}{\alpha_2} \times \left(\frac{\alpha_1}{x} - \frac{\alpha_3 x}{(x^2+\alpha_4^2)(1-x)}\right), \tag{32}$$

$$y_2(x) = \frac{x^2}{x^2+\beta_2 x+\beta_2\beta_1(1+L_0/I_c)}. \tag{33}$$

We write $\beta_0(I_c) = L_0/I_c$ here to exhibit the effect of $I_c$ explicitly, where $L_0 = l_{-0}/l_0$ is the dissociation constant for $IP_3$ binding. The null clines are shown in Fig. 5. The fast dynamics of the system are controlled by $y_1(x)$, which is a cubic-shaped curve. It has a single minimum and a single maximum in the domain of interest ($0 < x < 0.8$, $y > 0$). The minimum and maximum points ($x^{MIN}$, $y^{MIN}$) and ($x^{MAX}$, $y^{MAX}$), which we label MIN and MAX, respectively, separate the curve into three branches: the left branch (L), the middle branch (M), and the right branch (R). The curve for the slow dynamics is a simple monotonic curve that passes through (0, 0), and $\lim_{x\to\infty} y(x) = 1$. The two null clines have at least one intersection, but they can have at most three intersections.

The dynamics of $Ca_i$ are determined by the pattern of intersection of the null clines. When the $IP_3$ level is lower than 0.42 $\mu$M, the curve $y = y_2(x)$ intersects the curve $y = y_1(x)$ at three points: one in the L branch and two in the M branch. The first of these is a stable equilibrium point and

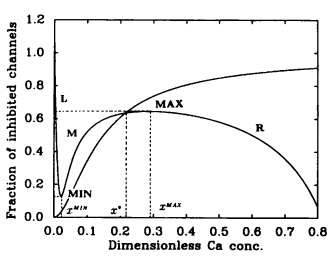


FIGURE 5 Null clines for Eq. 28. The intersection of $y_1$ and $y_2$ at ($x^*$, $y^*$) defines the equilibrium solution of the system, which is unstable in this case. The single intersection point $x^*$ is between $x^{MIN}$ and $x^{MAX}$, and the system has a stable periodic solution.

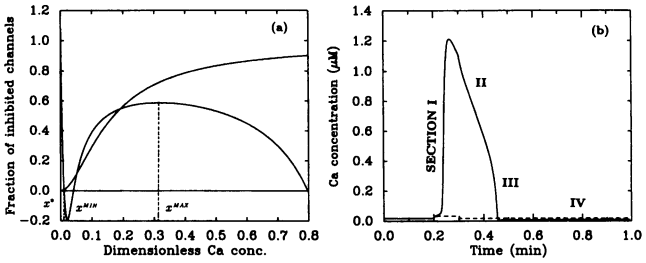


FIGURE 6 (*a*) Null clines for excitable responses, with $I_c = 0.3$ μM. The graph of $y_1(x)$ intersects that of $y_2(x)$ three times, but only the intersection with the lowest $x$ value is stable ($x^*$). (*b*) Superthreshold (*solid curve*) and subthreshold (*dashed curve*) responses in the time domain with $I_c = 0.3$ μM. A Ca flux of dimensionless amplitude 0.06 (subthreshold) and 0.07 (superthreshold) is applied for a duration of 0.1 min at 0.2 min. The superthreshold response is composed of the fast Ca upstroke, the slowly decaying component, the fast transition to a low level of $Ca_i$, and the slow recovery.

the $Ca_i$ is low, which corresponds to the normal resting state of the cell. The two equilibrium points on the M branch are unstable (see Fig. 6 *a*). At the stable steady state of low $Ca_i$, the system responds to perturbations in $IP_3$ or $Ca_i$ as an excitable system. The threshold value for an excitable response is determined by the M branch. If a perturbation carries the system state to the right of the M branch, then the solution first travels almost horizontally to the R branch, it follows the R branch until MAX, and then travels almost horizontally to the L branch. Once in the neighborhood of the L branch, it travels downward along the L branch until it returns to the stable equilibrium. In the time domain, this corresponds a large excursion in the $Ca_i$ before it returns to the low steady state. If the perturbation is subthreshold, the solution will return to the steady state without the large excursion; instead it first moves almost horizontally to the L branch and then travels to the stable equilibrium point along the L branch. A comparison of the time-dependent Ca responses to super- and subthreshold stimuli is shown in Fig. 6 *b*. The threshold value decreases as the $IP_3$ level increases.

## Ca oscillations and frequency encoding

When the $IP_3$ level exceeds 0.42 μM, the leftmost steady state lies between $x^{min}$ and $x^{max}$ for $IP_3$ not too large. The real parts of the eigenvalues of the linearized system at the steady-states are positive, and the system is oscillatory. The null clines and a computed trajectory for the periodic solution are shown in Fig. 7 *a*. The periodic solution for the corresponding degenerate system is composed of four segments: segment I, a rapid horizontal transition from MIN to the R branch; segment II, a slow solution evolution on the R branch to MAX; section III, another rapid horizontal transition, this time from MAX to the L branch; and section IV, a slow traversal of the L branch to the MIN point. One can see that the computed periodic orbit for the nondegenerate system depicted in this figure closely matches the degenerate orbit.

Figure 7 *b* and *c* also shows the time-dependent oscillatory solution using the dimensional variable $C_c = C_M x$ and $y = s_{111}$. By comparing the phase-plane curves of Fig. 7 *a* with the ones in the time domain in Fig. 7 *b* and *c*, one can see that, although the opening of channels produces the fast increase in Ca concentration, the inactivation of the channels determines the declining phase of the Ca spike. The time scale of channel closing is that of a single Ca spike. The slowest process in our model is the recovery of the channels from the inactivated state ($RIC^+C^-$), which is substantially longer than the time of a single Ca spike.

Bifurcation analysis shows how oscillatory solutions can arise in this system as $IP_3$ increases. Figure 8 shows the bifurcation diagram for this system. The periodic solution emerges by means of a homoclinic bifurcation at $IP_3 = 0.42$ μM and disappears at a Hopf point for $I_c = 1.42$ μM. One interesting aspect of calcium dynamics is that $IP_3$ stimuli are frequency encoded, as was discussed earlier. In the oscillatory range of $IP_3$ concentration, the oscillation frequency increases with increasing $IP_3$, while the change in the amplitude is not significant, as can be seen from Fig. 8. Time-domain responses that exhibit frequency encoding can be seen in Fig. 9 *b*. The reduction of the models to two equations makes the study of frequency encoding possible, as shown in Tang and Othmer (1995).

## Stable elevated $Ca_i$

As the $IP_3$ level is increased further, MIN is shifted upward (cf. Fig. 9 *a*) until the single intersection between $y_1(x)$ and $y_2(x)$ is on the R branch and the steady state is stable. For $I_c > 2.54$ μM this is the only stable solution of the system. A perturbation in $IP_3$ or Ca can displace the system from

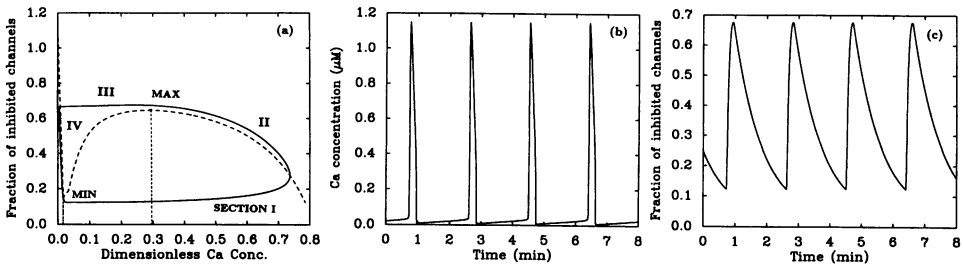


FIGURE 7 Closed orbit in the phase plane and a periodic solution in the time domain. (*a*) Null clines for a periodic solution with $I_c = 0.5$ and the corresponding phase-plane projection of the periodic solution. The periodic orbit for the corresponding degenerate solution with $\epsilon = 0$ is very close to this orbit. (*b*) Cytoplasmic calcium. (*c*) The fraction of channels in the inhibited state ($y = RIC^+C^-$).

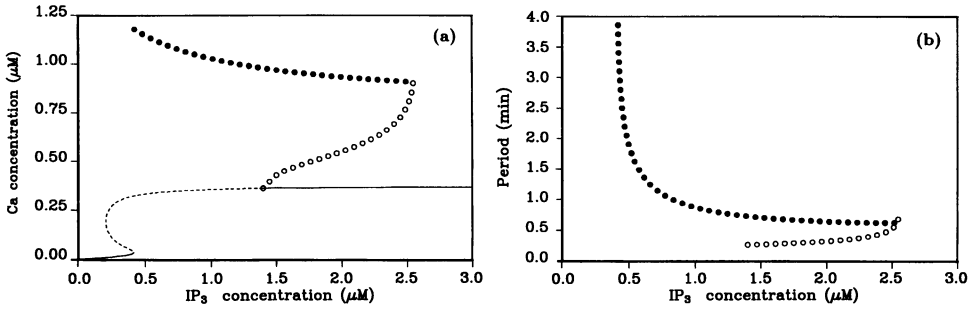


FIGURE 8 Effect of $IP_3$ on the behavior of the system. (*a*) The amplitude at steady state (*solid and dashed curves*) and the maximum amplitude of a periodic solution (*open and filled circles*) of Ca as a function of the $IP_3$ concentration. Solid curves and circles indicate stable solutions; dashed curves and open circles indicate unstable solutions. (*b*) The period in minutes of the periodic solutions in (*a*). These results were obtained with the software package AUTO (Doedel, 1986).

this equilibrium only temporarily, and the return to the steady state is rapid. This equilibrium differs from the stable equilibrium when $IP_3$ is small in that the $Ca_i$ concentration is much higher. This aspect is shown in the time domain in Fig. 9 *b*, where a simulation of several types of behavior of this system is shown. For comparison, the experimental results for endothelial cells under similar stimulus protocol are shown in Fig. 9 *c* (Jacob et al., 1988). This simulation shows how this simple model can simulate complex Ca dynamics quantitatively as well as qualitatively.

In the experiment, various concentrations of histamine were applied to the extracellular medium in the specific time periods shown in the lower trace in Fig. 9 *c*. One sees that there is a slight time delay between the Ca response and the application of histamine that is not captured in the simulation. This delay may be caused by signal transduction from the extracellular histamine increase to the increase in intracellular $IP_3$ in the neighborhood of $IP_3R$, which involves both the production of $IP_3$ in the membrane and its diffusion into the cytoplasm (Fig. 1). These steps are not included in the mathematical description at present.

## Effect of Ca exchange with the extracellular medium

The effect of slow Ca exchange with the extracellular medium on the intracellular Ca dynamics can be investigated in the reduced model through a change in $C_M$, the mean Ca concentration. This corresponds to a change in $C_M$ in the second equation of Eq. 27 or to a proportional change of the dimensionless parameters in Eq. 28 that are scaled by $C_M$, i.e., $\alpha_3$, $\alpha_4$, $\beta_1$, and $\beta_2$. Fig. 10 shows the bifurcation diagram with $I_c = 0.3$ $\mu$M and $C_M$ in the range 0–5 $\mu$M.

Suppose that initially $C_M = 0$, i.e., that there is no Ca in the ER-cytoplasm complex. If $C_M$ increases slowly with time, $Ca_i$ increases monotonically for $C_M < 1.90$ $\mu$M. When $C_M$ is close to 1.90 $\mu$M, the system is excitable and responsive to both $IP_3$ and Ca pulses. The threshold for an excitable response progressively decreases as $C_M$ approaches 1.90 $\mu$M from below, and at $C_M = 1.90$ $\mu$M a stable Ca oscillation ensues. This oscillation results from the gradual accumulation of intracellular Ca, not from an increase in $IP_3$ concentration. The maximal $Ca_i$ amplitude during an oscillation is 1.5 $\mu$M, which is significantly higher than that in Fig. 8 for $IP_3$-induced oscillations. As Ca

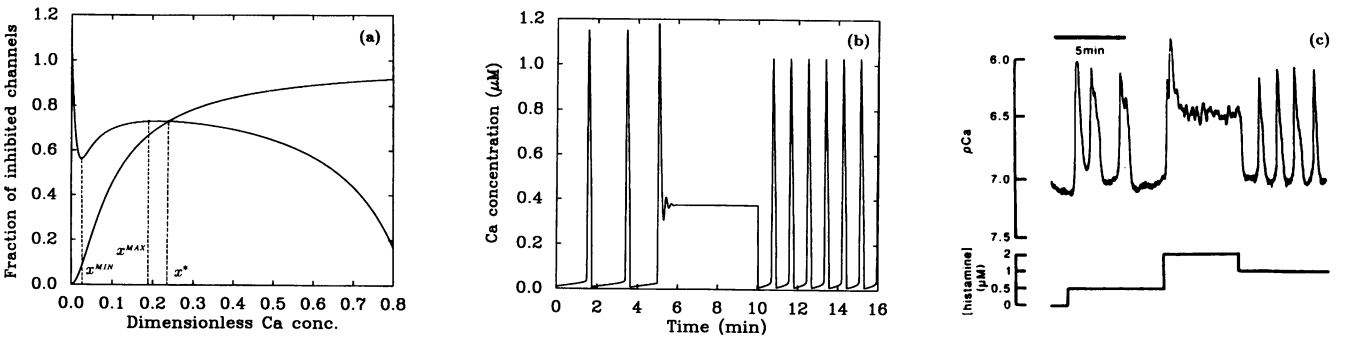


FIGURE 9 Null clines when $IP_3$ is high; $I_c = 5.0$ here. The dimensionless Ca value ($x^*$) is to the right of $x^{MAX}$, and the intersection point ($x^*$, $y^*$) is a stable equilibrium of the system. (*b*) The theoretically predicted calcium concentration, (*c*) the experimentally observed results for endothelial cells, reported in Jacob et al. (1988) (reproduced with permission). In (*b*) the $IP_3$ concentration is held at 0.5 $\mu$M for $T \in (0, 5$ min), then is increased to $IP_3 = 5.0$ $\mu$M for 5 min, and is held at $IP_3 = 1.0$ $\mu$M thereafter.

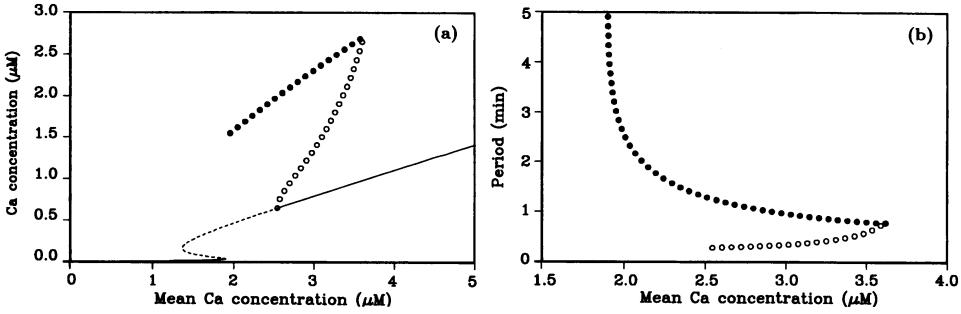


FIGURE 10 Effect of slow Ca exchange with the extracellular medium on intracellular Ca dynamics. (*a*) $Ca_i$ level (maximal Ca level for periodic solutions) as a function of $C_M$, the mean Ca concentration. Solid curves (circles) denote stable steady states (periodic solutions), and dashed curves (circles) denote unstable steady states (periodic solutions). $IP_3$ is 0.3 $\mu$M; (*b*) The corresponding period of the oscillatory solution as a function of $C_M$.

continues to enter the cell the oscillation increases in both amplitude and frequency, which is also different from the situation for $IP_3$-induced oscillations (Fig. 8), where $Ca_i$ decreases somewhat with increasing $IP_3$. The maximum $Ca_i$ amplitude is 2.7 $\mu$M and is attained at $C_M$ = 3.61 $\mu$M. When $C_M$ exceeds this value the cell is overstimulated and a stable elevated Ca level results. In further contrast to $IP_3$-induced overstimulation, as $C_M$ increases further, $Ca_i$ increases proportionally.

Fig. 10 can also be viewed from another perspective, i.e., when a cell placed in a Ca-free medium slowly loses Ca to the extracellular medium. If the cell is initially overloaded with Ca ($C_M > 3.61$ $\mu$M) the total amount of Ca in the ER-cytoplasm complex will slowly decrease and $Ca_i$ may begin to oscillate at $C_M$ = 3.61 $\mu$M. During each cycle the basal level of $Ca_i$ will decrease, and the oscillation will decrease in amplitude and frequency until $C_M$ drops below the lower limit of oscillations. Beyond this point $C_M$ will decrease monotonically until the cell has lost all its Ca.

In both Figs. 8 and 10 there is an interval in which a stable periodic solution coexists with a stable steady state. In Fig. 8 the interval is for $IP_3 \in$ [1.42 $\mu$M, 2.54 $\mu$M] with $C_M$ = 1.56 $\mu$M, and in Fig. 10 it is for $C_M \in$ [2.55 $\mu$M, 3.61 $\mu$M] with $IP_3$ = 0.3 $\mu$M. Theoretically the cell can remain in either state, depending on the initial condition, but this has apparently not been seen in experiments. The numerical simulations always lead to oscillatory solutions in the above regions, which suggests that the steady-state solutions have small domains of attraction in the phase plane, whereas the domains of attraction of the periodic orbits are large.

## Summary

We have studied the current models for the kinetics of $IP_3$-sensitive intracellular Ca channels. The different channel regulation schemes are shown to be reducible to a single gating equation that is linear in the gating variable and that has coefficients that depend on the $IP_3$ level and the $Ca_i$. The reduced model can reproduce the experimental data qualitatively and quantitatively. For example, the channel opening in response to changes in $\log_{10}$[Ca] at steady state is a bell-shaped curve. Dynamically, step increases in Ca can either activate or inhibit the channel, depending on the Ca levels before and after the increase. The channel also opens incrementally in response to step increases in $IP_3$. The reduction of different models to the same form makes the comparison among these models much easier. The form of the gating equations, which have only two or three parameters, can be used to identify the parameter values by fitting experimental data. Experimental tests to distinguish between the different schemes are provided.

For intracellular Ca dynamics, it is shown that the De Young–Keizer model and the Othmer–Tang model can be reduced to a standard form that involves two equations under the assumption that the total amount of intracellular Ca is conserved. Using a generic form based on the reduced Othmer–Tang model, we show that the simplified model predicts the excitability to pulse Ca and $IP_3$ stimuli at low $IP_3$ levels and results in Ca oscillations when the $IP_3$ concentration lies in a certain range. The oscillations show frequency encoding as the $IP_3$ concentration varies. The system responds to very high levels of $IP_3$ with damped oscillations and returns to a sustained elevated $Ca_i$ level.

A slow exchange of Ca between the cytoplasm and the extracellular medium can also be incorporated, and thus the theory is applicable when $J_m$ is small compared with the fluxes across the ER membrane. It is also applicable where a small artificial Ca influx or efflux is induced, as in anterior gonadotrophs when the membrane potential is clamped (Keizer and De Young, 1993). However, the theory is not applicable to certain cell types or certain experimental conditions in which there is significant Ca exchange between extracellular medium and cytoplasm. For example, in some neurons and in cardiac myocytes an autocatalytic depolarization of the membrane induces a rapid and massive Ca entry via Ca-specific or nonspecific channels (Tang and Othmer, 1994).

## Comparison with other simplified models

The Atri–Amundson–Clapham–Sneyd model does not have an equation for Ca dynamics in the ER because these authors assume that Ca in the ER is constant (Atri et al., 1993). In the De Young–Keizer model and the Othmer–Tang model the decrease in the Ca level in the ER is substantial; hence it cannot be neglected. Depending on the cell type in question, the Ca level in the ER can be depleted

by 10–100% as Ca is released during the spikes. Lo and Thayer (1993) showed that the Ca store is completely depleted with a single intermediate dosage of $IP_3$. Shuttleworth (1992) showed that the Ca leakage from the ER follows a single linear rate when $I_c = 0$, which implies that the driving force for Ca release decreases as Ca is released. When $I_c \neq 0$, the release through nonspecific leakage and $IP_3R$-specific release also follow a linear scheme (Oldershaw et al., 1991). These experimental data are consistent with the terms for Ca release used here, which are $P_r^{leak}(C_r - C_c)$ for nonspecific release and $P_r^{chan} s_{110}(C_r - C_c)$ for $IP_3R$-mediated Ca release.

Another difference between the Atri–Amundson–Clapham–Sneyd model and the reduction shown here stems from our assumption that the time scales for the channel dynamics and the Ca dynamics are sufficiently separated. We assume, based on evidence cited earlier, that the channel inhibition is relatively slow compared with that of the other Ca components, whereas in their model there is no significant difference in the time scales. The termination of Ca release in their model is caused by the inhibition of elevated $Ca_i$ on $IP_3R$, whereas in ours the major contributing factor is the decrease of Ca in the ER; the effect of $Ca_i$ inhibition of $IP_3R$ is secondary (cf. Fig. 7). We have tested the effects of decreasing the time scale of channel inhibition by increasing $\epsilon$. For instance, if $\epsilon = 1$ in the generic model, the inhibitory effect of $Ca_i$ on $IP_3R$ becomes dominant, as is in the Atri–Amundson–Clapham–Sneyd model. Although experimental data suggest a decoupling between the time scales (see above), the relative importance of these two factors in terminating of Ca release in a typical excitable response should be investigated further experimentally. It is possible that in some systems the inhibition of $IP_3R$ by $Ca_i$ occurs on the same time scale as for the other Ca components, in which case the reduced two-equation system can no longer be singularly perturbed. However, the phase-plane analysis employed here can still be applied.

A difference between the reduced Othmer–Tang model and the De Young–Keizer model is that the reduced equations for channel kinetics are different because the original channel schemes are different. Another important difference is that we are able to obtain frequency encoding in the reduced Othmer–Tang model, whereas no such property is reported for the reduced De Young–Keizer model. The decoupling of the time scales of channel inactivation and recovery is essential for achieving frequency encoding. In the reduced De Young–Keizer model, and in the Atri–Amundson–Clapham–Sneyd model, the time scale of the channel inactivation is about the same as for the channel recovery, which limits the amount of frequency modulation that can be achieved (Atri et al., 1993; De Young and Keizer, 1992; Li and Rinzel, 1994). In these two models the relaxation time of the low Ca state (channel recovery) is about the same as that for a single Ca spike. However, in cells showing significant frequency encoding, such as hepatocytes and endothelial cells, the time for a Ca spike is much shorter than that of the low $Ca_i$ recovery phase (Woods et al., 1986; Jacob et al., 1988). In Li and Rinzel (1994) and Atri et al. (1993) the Ca spikes increase in amplitude as the $IP_3$ level increases, whereas in our model the change in amplitude is very small (in fact the amplitude decreases slightly). To date, frequency encoding has been demonstrated only for the Othmer-Tang model; but based on the above analysis, it is possible that the reduced De Young–Keizer model reported here and that in Li and Rinzel (1994) may show frequency encoding as well for a different set of parameter values.

## Applications

The simplified models permit the application of techniques such as phase-plane analysis, which leads to a more detailed understanding of Ca dynamics. Theoretical studies on frequency encoding and on the effect of individual parameters can be carried out much more readily. The conditions for the existence and stability of traveling Ca waves, i.e., parameter domains and initiation thresholds, can be determined in the reduced model, and the relationship between channel properties and wave speed can be studied rigorously.

The simple model derived here can be used as a prototype for simulating more complex Ca dynamics in other systems. For example, Ca dynamics in the principal cells of the cortical collecting tubule regulate sodium and potassium transport across the epithelium. Ca is involved in the feedback control of the permeability of apical membrane to sodium and potassium (Taylor and Windhager, 1979; Wang et al., 1993). In the toad urinary bladder, Ca is involved in cell volume regulation (Wong and Chase, 1986). By utilizing the simplified model for Ca dynamics presented here, further insight into how $Ca_i$ is affected by and affects other factors in a cell can be gained.

In certain cell types there is evidence for the existence of both $IP_3$-induced calcium release through $IP_3R$ and Ca-induced Ca release through RyR. For example, rat chromaffin cells clearly show the coexistence of two types of calcium channels in the ER membrane (Malgaroli et al., 1990). In mouse pancreatic acinar cells, work by Wakui and others shows such coexistence as well (Wakui et al., 1989, 1990; Nathanson et al., 1992). Even in hepatocytes, Ca-induced Ca release through RyR may play a role in propagating a traveling calcium wave (Rooney et al., 1991). In the deutosome oocyte cells of certain species, both $IP_3R$ and the RyR have been shown to be involved in the propagation of the fertilization wave (Whitaker and Swann, 1993). Elsewhere, we will show that an analogous reduction for the kinetics of RyR can be carried out. Thus, the mathematical simplification of the kinetics for $IP_3R$ and the RyR will make it possible to study how these two distinct Ca channel types interact with each other in a propagating Ca wave.

This research is supported in part by NIH grant DK 31550 (to J. Stephenson) and by NIH grant GM 29123 (to H. Othmer).

**TABLE 4 Definitions of symbols**

| | |
|---|---|
| Subscripts | |
| $ijk$ | $IP_3R$ index with (1) or without (0) ligand; left to right sites; $I$, $C^+$, and $C^-$ |
| $i$, $r$ | Compartment, $i$ (cytoplasmic); $r$ (ER) |
| Dimensional Variable | |
| $C_c$ | Ca concentration in cytoplasm or on the *cis* side of a bilayer, $\mu$M |
| $C_r$ | Ca concentration in the ER, $\mu$M |
| $t$ | Time, s |
| Dimensionless Variables | |
| $\tau$ | Dimensionless time |
| $x$ | Dimensionless *cis* Ca concentration (channel kinetics) or $Ca_i$ |
| $y$ | Fraction of $IP_3R$ in the inhibited state |
| $y_i(x)$ | Null clines for the Ca dynamics (1) or channel gating (2) equation |
| $y_n$ | Gating variable (AACS) |
| $s_{ijk}$ | Fraction of $IP_3R$ in the $ijk$ state |
| $p_i$ | Probability of $IP_3R$ with $I$ (1), $C^+$ (2), and $(C^2)^-$ (3) bound (AACS) |
| $\tau_y$ | Time scale for gating variable $y$ |
| $y_\infty$ | Steady state of $y$ |
| Fluxes | |
| $J_m$ | Ca flux across the cytoplasmic membrane, $\mu$M/s |
| $J_r^{pump}$ | Ca flux carried by the ER Ca-ATPase, $\mu$M/s |
| $J_r^{chan}$ | Ca flux across the ER membrane through $IP_3R$, $\mu$M/s |
| $J_r^{leak}$ | Ca leakage flux across the ER membrane, $\mu$M/s |
| Kinetic constants | |
| $l_i$ | Binding rate of $I$ (0), $C^+$ (1), $C^-$ (2) to $IP_3R$, $(\mu M \cdot s)^{-1}$ |
| $\hat{l}_2$ | Binding rate of $(C^2)^-$ to $IP_3$ (AACS), $\mu M^{-2} \cdot s^{-1}$ |
| $l_{-i}$ | Off rate of $I$ (0), $C^+$ (1), $C^-$ (2) from $IP_3R$, $s^{-1}$ |
| $l_3$, $l_4$ | Binding rates of $I$ (3) or $C^-$ (4) to $IP_3R$ (DeY-K), $(\mu M \cdot s)^{-1}$ |
| $l_{-3}$, $l_{-4}$ | Off rate of $I$ (−3) or $C^-$ (−4) from $IP_3R$ (DeY-K), $s^{-1}$ |
| $l_r$ | Rate of $R^*IC^+ \rightarrow RIC^+C^-$ transition (B-E), $s^{-1}$ |
| $l_t$, $l_{-t}$ | Rate of $RIC^+ \rightarrow R^*IC^+$ transition or its reverse (B-E, B), $s^{-1}$ |
| $L_0$ | Dissociation constant for $IP_3$ binding ($l_{-0}/l_0$), $\mu$M |
| Other constants | |
| $\tau_n$ | Time constant for gating variable $y_n$ (AACS), s |
| $C_M$ | Reference or mean Ca concentration in cytoplasm-ER complex, $\mu$M |
| $I_c$ | $IP_3$ concentration in the cytoplasm, $\mu$M |
| $K_r^M$ | Michaelis–Menten constant for ER Ca-ATPase, $\mu$M |
| $P_r^{leak}$ | ER membrane permeability, 1/s |
| $P_r^{max}$ | Maximal active Ca flux, $\mu$M/s |
| $n$ | Hill coefficient for the ER Ca-ATPase, dimensionless |
| $v_r$ | Volume ratio of the ER to the cytoplasm, dimensionless |
| $z_r$ | Molar fraction of Ca inside ER (B-E), dimensionless |
| Special points | |
| $(x^{max}, s_{110}^{max})$ | Maximal point of steady-state Ca versus $RIC^+$, dimensionless |
| $(x^*, y^*)$ | Intersection point of null clines on the phase plane, dimensionless |
| $(x^{MIN}, y^{MIN})$ | Minimal point of the null cline $y_1(x)$, dimensionless |
| $(x^{MAX}, y^{MAX})$ | Maximal point of the null cline $y_1(x)$, dimensionless |

## APPENDIX: VALUES OF DIMENSIONAL PARAMETERS

The values of the dimensional parameters for the Bezprozvanny–Ehrlich model (B-E), the Othmer–Tang model (O-T), and the De Young–Keizer model (DeY-K) are given in Table 3, and their definitions and those of the Atri–Amundson–Clapham–Sneyd model (AACS) are given in Table 4. Some values for the parameters are recalculated from their original values to conform to the symbol usage here. For the justification and estimation of parameter values in these models, the reader should refer to the original papers.

## REFERENCES


Atri, A., J. Amundson, D. Clapham, and J. Sneyd. 1993. A single-pool model for intracellular calcium oscillations and waves in the *Xenopus laevis* oocyte. *Biophys. J.* 65:1727–1739.

Berridge, M. J. 1990. Inositol 1,4,5-trisphosphate-induced calcium mobilization is localized in *Xenopus* oocytes. *Proc. R. Soc. London Ser. B.* 238:235–343.

Bezprozvanny, I. 1994. Theoretical analysis of calcium wave propagation based on inositol (1,4,5)-trisphosphate ($InsP_3$) receptor functional properties. *Cell Calcium.* 16:151–166.

Bezprozvanny, I., and B. Ehrlich. 1994. Inositol (1,4,5)-trisphosphate ($InsP_3$)-gated Ca channels from cerebellum: conduction properties for divalent cations and regulation by intraluminal calcium. *J. Gen. Physiol.* 104:821–856.

Bezprozvanny, I., J. Watras, and B. E. Ehrlich. 1991. Bell-shaped calcium-response curves of $Ins(1,4,5)P_3$- and calcium-gated channels from endoplasmic reticulum of cerebellum. *Nature (London).* 351:751–754.

Boitano, S., E. R. Dirksen, and M. J. Sanderson. 1992. Intercellular propagation of calcium waves mediated by inositol trisphosphate. *Science.* 258:292–295.

De Young, G., and J. Keizer. 1992. A single-pool inositol 1,4,5-trisphosphate-receptor-based model for agonist-stimulated oscillations in $Ca^{+2}$ concentration. *Proc. Natl. Acad. Sci. USA.* 89:9895–9899.

Doedel, E. 1986. AUTO: Software for continuation and bifurcation problems in ordinary differential equations. Tech. Rept. California Institute of Technology.

Ehrenstein, G., and R. FitzHugh. 1986. A channel model for development of the fertilization membrane in sea urchin eggs. *In* Ionic Channels in Cells and Model Systems. R. Latorre, editor. Plenum Press, New York. 421–430.

Fay, F., S. Gilbert, and R. Brundage. 1995. Calcium signalling during chemotaxis. *In* Calcium Waves, Gradients and Oscillations, Ciba Foundation Symposium 188. John Wiley & Sons, Chichester. 121–145.

Finch, E. A., T. J. Turner, and S. M. Goldin. 1991. Calcium as a coagonist of inositol 1,4,5-triphosphate-induced calcium release. *Science.* 252: 443–446.

Gmaj, P., and H. Murer. 1988. Calcium transport mechanisms in epithelial cell membranes. *Miner. Electrol. Metab.* 14:22–30.

Goldbeter, A., G. Dupont, and M. J. Berridge. 1990. Minimal model for signal-induced Ca oscillations and for their frequency encoding through protein phosphorylation. *Proc. Natl. Acad. Sci. USA.* 87:1461–1465.

Gorelova, N., and J. Bures. 1983. Spiral waves of spreading depression in the isolated chicken retina. *J. Neurobiol.* 14:353–363.

Gyorke, S., and M. Fill. 1993. Ryanodine receptor adaptation: Control mechanism of $Ca^{2+}$-induced $Ca^{2+}$ release in heart. *Science.* 260: 807–809.

Hirose, K., and Iino, M. 1994. Heterogeneity of channel density in inositol-1,4,5 trisphosphate-sensitive $Ca^{2+}$ stores. *Nature (London).* 372: 791–794.

Hodgkin, A. L., and A. F. Huxley. 1952. A quantitative description of membrane current and application to conduction and excitation in nerve. *J. Physiol.* 117:500–544.

Iino, M., and M. Endo. 1992. Calcium-dependent immediate feedback control of inositol 1,4,5-trisphosphate-induced $Ca^{2+}$ release. *Nature (London).* 360:76–78.

Irvine, R. F. 1990. Quantal $Ca^{2+}$ release and the control of $Ca^{2+}$ entry by inositol phosphates—a possible mechanism. *FEBS.* 263:5–9.

Jacob, R., J. Merritt, T. Hallam, and T. Rink. 1988. Repetitive spikes in cytoplasmic calcium evoked by histamine in human endothelial cells. *Nature (London).* 335:40–45.

Kasai, H. 1995. Pancreatic calcium waves and secretion Ciba Foundation Symposium 188. Calcium Waves, Gradients and Oscillations. Chichester: John Wiley & Sons. pp 104–120.

Keizer, J., and G. De Young. 1993. Effect of voltage-gated plasma membrane $Ca^{2+}$ fluxes on $ip_3$-linked $Ca^{2+}$ oscillations. *Cell Calcium* 14: 397–410.

Keizer, J., and G. De Young. 1994. Simplification of a realistic model of $IP_3$-induced $Ca^{2+}$ oscillations. *J. Theor. Biol.* 166:431–442.

Kijima, H., and S. Kijima. 1983. Steady/equilibrium approximation in relaxation and fluctuation II. Mathematical theory of approximation in first-order reaction. *Biophy. Chem.* 17:261–283.

Koster, H., C. van Os, and R. Bindels. 1993. $Ca^{2+}$ oscillations in the rabbit renal cortical collecting system induced by $Na^+$ free solutions. *Kidney Int.* 43:828–836.

Lechleiter, J., and D. Clapham. 1992. Molecular mechanisms of intracellular calcium excitability in *X. laevis* oocytes. *Cell.* 69:283–294.

Lechleiter, J., S. Girard, E. Peralta, and D. Clapham. 1991. Spiral calcium wave propagation and annihilation in *Xenopus laevis* oocytes. *Science.* 252:123–126.

Li, Y., and J. Rinzel. 1994. Equations for $InsP_3$ receptor-mediated $Ca^{2+}$ oscillations derived from a detailed kinetic model: a Hodgkin–Huxley like formalism. *J. Theor. Biol.* 166:461–473.

Lo, T., and S. Thayer. 1993. Refilling the inositol 1,4,5-trisphosphate-sensitive $Ca^{2+}$ store in neuroblastoma × glioma hybrid NG108–15 cells. *Am. J. Physiol.* 264:C641–C653.

Lupu-Meiri, M., H. Shapira, and Y. Oron. 1988. Hemispheric asymmetry of rapid chloride responses to inositol trisphosphate and calcium in *Xenopus* oocytes. *FEBS Lett.* 240:83–87.

Malgaroli, A., R. Fesce, and J. Meldolesi. 1990. Spontaneous $[Ca^{2+}]_i$ fluctuations in rat chromaffin cells do not require inositol 1,4,5-trisphosphate elevations but are generated by a caffeine- and ryanodine-sensitive intracellular $Ca^{2+}$ store. *J. Biol. Chem.* 265:3005–3008.

Meyer, T. 1991. Cell signaling by second messenger waves. *Cell.* 64: 675–678.

Meyer, T., and L. Stryer. 1988. Molecular model for receptor-stimulated calcium spiking. *Proc. Natl. Acad. Sci. USA.* 85:5051–5055.

Meyer, T., and L. Stryer. 1990. Transient calcium release induced by successive increments of inositol 1,4,5-trisphosphate. *Proc. Natl. Acad. Sci. USA.* 87:3841–3845.

Meyer, T., and L. Stryer. 1991. Calcium spiking. *Ann. Rev. Biophys. Biophys. Chem.* 20:153–174.

Nathanson, M., P. Padfield, A. O'Sullivan, A. Burgstahler, and J. Jamieson. 1992. Mechanism of $Ca^{2+}$ wave propagation in pancreatic acinar cells. *J. Biol. Chem.* 267:18118–18121.

Nedergaad, M. 1994. Direct signaling from astrocytes to neurons in cultures of mammalian brain cells. *Science.* 263:1768–1771.

Nuccitelli, R. 1991. How do sperm activate eggs? *Curr. Top. Dev. Biol.* 25:1–16.

Oldershaw, C., D. Nunn, and C. Taylor. 1991. Quantal $Ca^{2+}$ mobilization stimulated by inositol 1,4,5-trisphosphate in permeabilized hepatocytes. *Biochem. J.* 278:705–708.

Othmer, H., and Y. Tang. 1993. Oscillations and waves in a model of calcium dynamics. *In* Experimental and Theoretical Advances in Biological Pattern Formation. H. Othmer, J. Murray, and P. Maini, editors. Plenum Press, London. 295–319.

Parker, I., and I. Ivorra. 1990. Inhibition by Ca of inositol trisphosphate-mediated Ca liberation: a possible mechanism for oscillatory release of Ca. *Proc. Natl. Acad. Sci. USA.* 87:260–264.

Rooney, T. A., D. C. Renard, E. J. Sass, and A. P. Thomas. 1991. Oscillatory cytosolic calcium waves independent of stimulated inositol 1,4,5-trisphosphate formation in hepatocytes. *J. Biol. Chem.* 266: 12272–12282.

Shuttleworth, T. 1992. $Ca^{2+}$ release from inositol trisphosphate-sensitive stores is not modulated by intraluminal $[Ca^{2+}]$. *J. Biol. Chem.* 267: 3573–3576.

Sneyd, J., A. Charles, and M. Sanderson. 1994. A model of the propagation of intercellular calcium waves. *Am. J. Physiol.* 266:C293–C302.

Tang, Y. 1993. Theoretical Studies on Second Messenger Dynamics. University Microfilms, Inc., Ann Arbor, MI.

Tang, Y., and H. Othmer. 1994. A model of calcium dynamis in cardiac myocytes based on the kinetics of ryanodine-sensitive calcium channels. *Biophys. J.* 67:2223–2235.

Tang, Y., and H. Othmer. 1995. Frequency encoding in excitable systems and its application to calcium oscillations. *Proc. Natl. Acad. Sci. USA.* 92:7869–7873.

Tang, Y., and J. Stephenson. 1995. Calcium dynamics and homeostasis in a mathematical model of the principal cell of the cortical collecting tubule. *J. Gen. Physiol.* (In press).

Taylor, A., and E. Windhager. 1979. Possible role of cytosolic calcium and Na–Ca exchange in regulation of transepithelial sodium transport. *Am. J. Physiol.* 236:F505–512.

Taylor, C. W., and B. V. L. Potter. 1990. The Size of inositol 1,4,5-trisphosphate-sensitive Ca stores depends on inositol 1,4,5-trisphosphate concentration. *Biochem. J.* 266:189–194.

Thastrup, O., P. Cullen, B. Drobak, M. Hanley, and A. Dawson. 1990. Thapsigargin, a tumor promoter, discharges intracellular $Ca^{2+}$ stores by specific inhibition of the endoplasmic reticulum $Ca^{2+}$ ATPase. *Proc. Natl. Acad. Sci. USA.* 87:2466–2470.

Thomas, A. P., D. C. Renard, and T. A. Rooney. 1991. Spatial and temporal organization of calcium signalling in hepatocytes. *Cell Calcium.* 12:111–126.

Tikhonov, A. 1952. Systems of differential equations containing small parameters multiplying derivatives. *Mathem. Sb.* 31:575–586.

Wakui, M., Y. V. Osipchuk, and O. H. Petersen. 1990. Receptor-activated cytoplasmic Ca spiking mediated by inositol trisphosphate is due to Ca-induced Ca release. *Cell.* 63:1025–1032.

Wakui, M., and O. H. Petersen. 1990. Cytoplasmic Ca oscillations evoked by acetylcholine or intracellular infusion of inositol trisphosphate or Ca can be inhibited by internal Ca. *FEBS Lett.* 263:206–208.

Wakui, M., B. V. L. Potter, and O. H. Petersen. 1989. Pulsatile intercellular calcium release does not depend on fluctuations in inositol trisphosphate concentrations. *Nature (London).* 339:317–320.

Wang, W., J. Geibel, and G. Giebisch. 1993. Mechanism of apical $K^+$ channel modulation in principal renal tubule cells. *J. Gen. Physiol.* 101:673–694.

Watras, J., I. Bezprozvanny, and B. E. Ehrlich. 1991. Inositol 1,4,5-trisphosphate-gated channels in cerebellum: presence of multiple conductance states. *J. Neurosci.* 11:3239–3245.

Whitaker, M., and K. Swann. 1993. Lighting the fuse at fertilization. *Development.* 117:1–12.

Wong, S., and H. Chase, Jr. 1986. Role of intracellular calcium in cellular volume regulation. *Am. J. Physiol.* 250:C841–C852.

Woods, N. M., K. S. R. Cuthberson, and P. H. Cobbold. 1986. Repetitive transient rises in cytoplasmic free calcium in hormone-stimulated hepatocytes. *Nature (London).* 319:600–602.

Wootton, J., J. Corrie, T. Capiod, J. Feeney, D. Threntham, and D. Ogden. 1995. Kinetic of cytosolic $Ca^{2+}$ concentration after photolytic release of 1-D-inositol 1,4-bisphosphate 5-phosphorothioate from a caged derivative in guinea pig hepatocytes. *Biophys. J.* 68:2601–2607.

Zhao, H., P. A. Loessberg, G. Sachs, and S. Muallem. 1990. Regulation of intracellular $Ca^{2+}$ oscillation in AR42J Cells. *J. Biol. Chem.* 265: 20856–20862.